博士学位論文

Hox及びその標的遺伝子による位置固有な四肢骨分化機構の解明

名古屋大学　大学院理学研究科　生命理学専攻

山本　詩織

Contents

Abstract_____1

Abbreviations_____3

Introduction_____4

Materials and Methods_____8

Results_____17

Discussion_____73

Acknowledgements_____96

References_____97

Table legends_____105

Abstract

To elucidate the role of *Hox* genes in limb cartilage development the target genes of HOXA11 and HOXA13 were identified by ChIP-Seq. The ChIP DNA fragment contained evolutionarily conserved sequences and multiple highly conserved HOX binding sites. A substantial portion of the HOXA11 ChIP fragment overlapped with the HOXA13 ChIP fragment indicating that both factors share common targets. Deletion of the target regions neighboring *Bmp2* or *Tshz2* reduced their expression in the autopod suggesting that they function as the limb bud-specific enhancers. The *Hox* downstream genes were identified as exhibiting expression changes in the *Hoxa13* knock out (KO) and *Hoxd11-13* deletion double mutant (*Hox13* dKO) autopod by Genechip analysis. The *Hox* downstream genes neighboring the ChIP fragment were defined as the direct targets of *Hox*. The spatial expression pattern of the *Hox* target genes that encode two different categories of transcription factors was analyzed during autopod development and *Hox13*dKO limb bud. (1) *Bcl11a*, encoding a repressor of cartilage differentiation, was expressed in the E11.5 autopod and was substantially reduced in the *Hox13*dKO. (2) The transcription factors *Aff3*, *Bnc2*, *Nfib* and *Runx1t1* were expressed in the zeugopodal cartilage but not in the

autopod due to the repressive or relatively weak transcriptional activity of *Hox13* at E11.5. Interestingly, the expression of these genes was later observed in the autopodal cartilage at E12.5. These results indicate that *Hox13* transiently suspends the cartilage differentiation in the autopodal anlage via multiple pathways until establishing the paddle-shaped structure required to generate five digits.

Abbreviations

ChIP: Chromatin immunoprecipitation

ChIP-Seq: ChIP-sequencing

HBS: HOX binding sequence

KO: knock out

PCR: polymerase chain reaction

Introduction

The tetrapod free limb is subdivided into three anatomical domains along the proximodistal axis: the stylopod, zeugopod and autopod. These domains possess a specific number and pattern of the bones and each bone possesses a unique morphology and length. During limb development, the mesenchymal cells of the limb bud first form precartilaginous aggregates which eventually grow and differentiate into the limb cartilage(Gilbert and Barresi 2016). The process occurs sequentially in the proximal to distal direction with the growth of the limb bud. Expression of *Hox* genes belonging to the *Abd-B* family, *Hox9-13*, is closely related to the anatomical domains of the limb bones (Izpisua-Belmonte et al. 1991;Yokouchi et al. 1991) and crucial for controlling morphogenesis and patterning of the limb cartilage (Pineault and Wellik 2014). *Hoxa11* and *Hoxd11* show overlapping expression in the zeugopodal mesenchyme and simultaneous loss of function of both genes in the forelimb bud results severe truncation of the zeugopodal bones without affecting the other long bones (Davis et al. 1995;Boulet and Capecchi 2004). *Hoxa13* and *Hoxd13* are expressed in the autopodal mesenchyme

and double knockout (KO) mice have smaller autopods during the embryonic stage and there was almost no sign of cartilage patterning in the entire autopod (Fromental-Ramain et al. 1996). These double homozygous KO mice exhibited much more severe phenotypes than single homozygous KOs suggesting that the paralogous genes are functionally redundant (Davis et al. 1995;Fromental-Ramain et al. 1996). A further role for *Hox* in domain-specific cartilage development was shown by misexpression of *Hox* in the limb mesenchyme. Viral or genetic misexpression of *Hoxa13* or *Hoxd13* in the zeugopodal mesenchyme repressed cartilage differentiation and proliferation resulting in zeugopod-specific cartilage truncation (Yokouchi et al. 1995;Goff and Tabin 1997;Peichel et al. 1997). Thus, *Hox* genes are expressed in a domain-specific manner in the limb bud mesenchyme and have a crucial function in domain-specific cartilage morphogenesis. Since *Hox* encodes a transcription factor, *Hox* target genes function in region/compartment-specific formation of the precartilaginous condensation, cellular differentiation and proliferation of the cartilage.

In contrast, *Hox* genes also control the expression of *Fgf10* in the distal limb

mesenchyme and *Shh* in the posterior mesenchyme to regulate limb outgrowth and proper supply of mesenchymal cells in coordination with the developmental time course of the limb bud (Kmita et al. 2005;Capellini et al. 2006;Sheth et al. 2013). How this growth control system coordinates with the domain-specific cartilage pattern formation system is an important question that remains to be resolved.

In order to understand the system that determines domain-specific limb cartilage development, it is essential to identify the direct *Hox* target genes. While limited numbers of *Hox* downstream genes have been reported, the known function of these genes does not sufficiently explain the *Hox* loss-of-function phenotype (McCabe and Innis 2005;Salsi and Zappavigna 2006). Recently the *Hox* target genes in the limb bud were exhaustively identified by ChIP-Seq analysis which opened the door to elucidate the function of the *Hox* genes in region-specific cartilage development (Sheth et al. 2016;Jerkovic et al. 2017). Since *Hox11* and *Hox13* control the growth and cartilage differentiation of the zeugopod and autopod, respectively, questions were raised if they share common targets, and if so, how the common targets are differentially regulated to give rise to domain-specific

morphology. To this end, the target genes of HOXA11 and HOXA13 in the limb bud were identified by ChIP-Seq analysis. It was found that they share common target sequences that contain multiple evolutionarily conserved HOX binding sites and the representative target sequences possess limb-bud specific enhancer functions. It was also found that common target genes expressed in the mesenchyme and developing cartilage exhibited differential control by HOXA11 and HOXA13 that may explain the unique autopodal cartilage developmental program.

Materials and Methods

Animal experimentation

This study was approved by the Institutional Animal Care and Use Committee of the Graduate School of Science and carried out according to the Nagoya University Animal Experimentation Regulations. The *Hoxa13* targeted mice (Fromental-Ramain et al. 1996) were obtained from Dr. Pierre Chambon. The $HoxD^{del(11-13)}$ allele (Zakany et al. 1997) and the *Ulnaless* (Peichel et al. 1997) were provided by Dr. Denis Duboule. Noon on the day the vaginal plug was observed was considered as E0.5. The embryos were isolated by caesarean incision and genotype was assessed by PCR.

Chromatin immunoprecipitation (ChIP)

Production of the anti-HOXA13 antibody was described previously (Yokouchi et al. 1995). The method for production and purification of the anti-HOXA11 antibody was also previously described (Yamamoto et al. 1998). The antibodies used in the present study were prepared from rabbits. ChIP was performed according to a standard protocol (Green

and Sambrook 2012) with the following modifications. Whole limb buds from E11.5 and the autopod from E11.0 wild-type ICR mice were dissected in ice-cold PBS. Embryonic tissues were homogenized 13 times with a tight-fitting Dounce homogenizer, then fixed in 1% formaldehyde/PBS for 10 minutes at 4 °C and quenched with 0.1 M glycine. The cross-linked material was sonicated to produce 200-1000 bp fragments with a DNA Shearing System S2 (Covaris). The immunoprecipitations were performed with 11 pairs of autopods from E11.0 embryos or 12-18 pairs of whole limb buds from E11.5 embryos. Pierce™ Protein A/G magnetic beads (Thermo Scientific) were conjugated with 10 µg of anti-HOXA13 (Yokouchi et al., 1995) or 8 µg of anti-HOXA11. Sonicated chromatin was incubated with the antibody-protein A/G beads complex overnight at 4°C with rotation. ChIP DNA fragments and control input DNA fragments were converted to a sequence library by NEB Next Ultra™ DNA Library Prep kit for Illumina (NEB) then analyzed by using a HiSEQ 1500 (Illumina). E12.5 ChIP-Seq was performed as described previously (Beccari et al. 2016). For data analysis of E12.5 ChIP-Seq, distal ChIP data and proximal ChIP data were combined. HOXA13 ChIP sequence data were analyzed by Bowtie 2.2.2

(Langmead and Salzberg 2012) and MACS 2.1.0 (Zhang et al. 2008) (mm9) organized by SraTailor (Oki et al. 2014) under default parameters except 2.15e09 was used for the mouse genome size. For the analysis of HOXA11 ChIP-Seq by MACS2.1.0 (mm9), the following parameters were used: --nomodel, --extsize 200, -g 2.15e09. NGS sequence data of input DNA without ChIP was used as the reference. Overlapping of the ChIP peaks was determined by Bed Tools/ Intersect intervals (Quinlan and Hall 2010) via Galaxy (Giardine et al. 2005). ComputeMatrix/NGS: DeepTools and plotHeatmap/NGS: DeepTools (Ramirez et al. 2016) in Galaxy were used for creating the aggregate plot. To analyze the sequence conservation around the HOX ChIP summit, the bed file in mm9 format was first converted to mm10 format using the LiftOver tool of the USCE genome browser (Karolchik et al. 2004) then analyzed with the same method used to prepare the aggregate plot using mm10.60way.phastCons.bw data obtained from the UCSC genome browser. For the analysis of sequence motif enrichment, the genomic spans given in BED format were first converted to FASTA files using UCSC Table Browser then analyzed by

MIME-ChIP (Machanick and Bailey 2011). ChIP-Seq data have been deposited in the Gene Expression Omnibus (GEO) with accession number GSE119142.

Data analysis

Integrative genome viewer, IGV_2.4.3 (Robinson et al. 2011), was used for graphical analysis of the ChIP-Seq data. Data analysis was also performed using the online application provided by CEAS (Shin et al. 2009) for positioning the ChIP DNA fragments relative to the gene structure, David ver. 6.8 (Huang da et al. 2009) and Panther ver. 13.1 (Mi et al. 2013) for enrichment analysis and classification of the genes, Venny (http://bioinfogp.cnb.csic.es/tools/venny/) for listing common genes in different gene pools, or GREAT (McLean et al. 2010) through the UCSC Genome Browser for identification of the genes neighboring the ChIP peak using a default parameter. Data sets obtained from the public databases are shown in Table 6.

Genechip

Embryos isolated approximately E11.25 were preserved in RNA later (Ambion) and the autopodal tissue corresponding to the *Hoxd13* expressing region was dissected. Total RNA was isolated using the RNeasy Mini Kit (QIAGEN) and biotin labeled RNA was prepared using the IVT Labeling Kit (Affymetrix), One-Cycle cDNA Synthesis Kit (Affymetrix) and Sample Cleanup Modules (Affymetrix). The GeneChip Mouse Genome 430 2.0 Array (Affymetrix) were hybridized, washed, stained and scanned by using standard Affymetrix GeneChip reagents and protocols. Data from two independent experiments were analyzed using the Affymetrix Transcriptome Analysis Console V3.0. Genechip data have been deposited in the GEO with accession number GSE118640. Genes exhibiting more than a 1.5-fold change in the expression ($P<0.05$) were defined as the HOX13 downstream genes. This study was done by Tomomi Ohtani in this laboratory.

***In situ* hybridization**

Whole-mount *in situ* hybridization (WISH) was performed as previously described

(Yamamoto-Shiraishi and Kuroiwa 2013). Digoxigenin (DIG) or fluorescein-labeled riboprobes were synthesized using the template cDNA fragments amplified with the primer sets listed in Table 5e directly or after cloning into plasmids. Template cDNA clone for the mouse *Hoxd13* probe was provided by Dr. D. Duboule. Generation of the *Bmp2* probe was described previously (Dickinson et al. 1990). Samples were photographed with a Nikon DXM1200F camera system, and the background color was adjusted to obtain best contrast to the signals in each sample. For comparison of the signal patterns between limbs, some limb photographs were flipped horizontally using Adobe Photoshop CS6.

Electrophoresis mobility shift assay (EMSA).

The protein coding sequence containing homeobox in the second exon was PCR amplified using the primers presented in Table 5a and connected to the sequence encoding the Maltose binding protein (MBP) in pMal-c (NEB). Protein production and affinity purification was performed according to the manufacturer's instructions (NEB). For preparing the fluorescently labeled probes, aminoallyl-labeled double strand DNA was

prepared by two-step PCR. The first round of PCR was done using mouse genomic DNA template and RVL-GSP1 and GSP2 primers. This PCR product was then used as the template for the second round of PCR using aminoallyl-RVL and GSP2 as primers. The sequence of each primer is shown in Table 5b. The aminoallyl-labeled DNA fragments were reacted with Alexa Fluor 700 (AF700) NHS ester (Thermo Fisher) in borate buffer then purified using the Qiagen MinElute column (Qiagen). The sequences of the unlabeled competitors are presented in Table 5c. For the EMSA reaction (25 µl), 0.5 pmoles of AF700 labeled probe was mixed with MBP or MBP-mHOXA11 (or13) HD protein in buffer containing 1 µg poly (dIdC), 20 mM TrisHCl pH 7.5, 150 mM KCl, 0.1% Triton X-100, 1 mM EDTA, 1 mM DTT and 5% glycerol for 30min at 25°C. After adding 1 µl of 0.05% bromophenol blue solution, the reaction was analyzed by 2% low melting point agarose gel electrophoresis at 4°C using 0.5x TBE as the running buffer. The gel was analyzed with an Odyssey scanner (LI-CORE). For competition experiments, 2.5 pmoles or 25 pmoles of the oligo nucleotides were added to the reaction.

Deletion of specific chromosomal regions

Mice with deletion of the putative enhancer of *Tshz2* or *Bmp2* were generated using the CRISPR/Cas9-based genome editing system via electroporation (Hashimoto et al. 2016). The guide RNA sequences and deleted regions are presented in Table 5d.

Micromass culture and transfection

For micromass culture (MMC), mesenchymal cells of the distal limb bud were prepared as previously described (Yamamoto-Shiraishi et al. 2014), except Dispase I (WAKO) was used instead of trypsin (final concentration of dispase: 2000U/ml). For transfection of MMC, 0.9 μl FuGENE HD (Promega) was mixed with 4.4 μl F-12 and 300 ng plasmid DNA (containing 100 ng pCAGGS-*H2B-EGFP*, and 200 ng pCAGGS, pCAGGS-mouse *Bcl11a*, or pCAGGS-mouse *Bcl11b*, respectively). After incubation for 20 min, 13.2 μl cell suspension (2.5×10^7 cells/ml) containing 2% FBS was added, and cells were seeded onto a glass base dish (ø = 3.5 cm). After incubation in 5% CO_2 at 37°C for 2 h, 10% FBS/F-12 was added (1 ml/dish). Medium was changed every day. After the incubation for 1 or 2

days, MMCs were fixed with 4% PFA/0.1% Tween20/PBS. Anti-Collagen II Ab-2, mouse monoclonal Ab (NeoMarkers, MS-235; dilution: 1/200) and goat anti-mouse IgG (H+L), Alexa Fluor 594 (Thermo Fisher, A-11032; dilution: 1/300) were used as primary and secondary antibodies, respectively. Nuclear staining was performed with DAPI, and MMCs were photographed using a M205FA (Leica) and FV1000 (Olympus). Col II immunofluorescence signal intensity around each nucleus was calculated using Image J. cDNA fragments encoding the mouse *Bcl11a* and *Bcl11b* protein coding sequence were amplified from reverse transcripts of E11.5 limb bud RNA using primer sets presented in Table 5f and were cloned into the pCAGGS vector.

Results

Hoxa11 and *Hoxa13* have distinctive expression domains in the limb bud

Hoxa11 and *Hoxa13* show unique expression pattern along the proximodistal axis in the mesenchyme of the E11.75 mouse forelimb bud (Fig. 1A and B). At this stage of limb development, formation of the zeugopodal cartilage anlage is complete and the carpal and metacarpal precartilaginous condensations are already visible in a continuous anlage of the autopodal region (Fig. 1E). Correlations between the *Hox* expression domain and the cartilage patterning were examined by double staining for the expression of *Hox* and the cartilage marker *Col2a1* (Fig. 1C and D). As shown in Fig.1C and 1F, *Hoxa11* is expressed in the distal zeugopodal region and proximal autopodal region spanning most of the carpal cartilaginous condensation. In contrast, *Hoxa13* is expressed throughout the entire autopodal region (Fig. 1D and G). Thus, expression of *Hoxa11* and *Hoxa13* covers different domains along the proximodistal axis and overlaps around their expression boundary corresponding to the carpal cartilage anlage (Fig. 1H). This same topological correlation between *Hox* expression and cartilage patterning was observed in the E11.75

hindlimb bud (Fig. 2A-G).

Figure 1

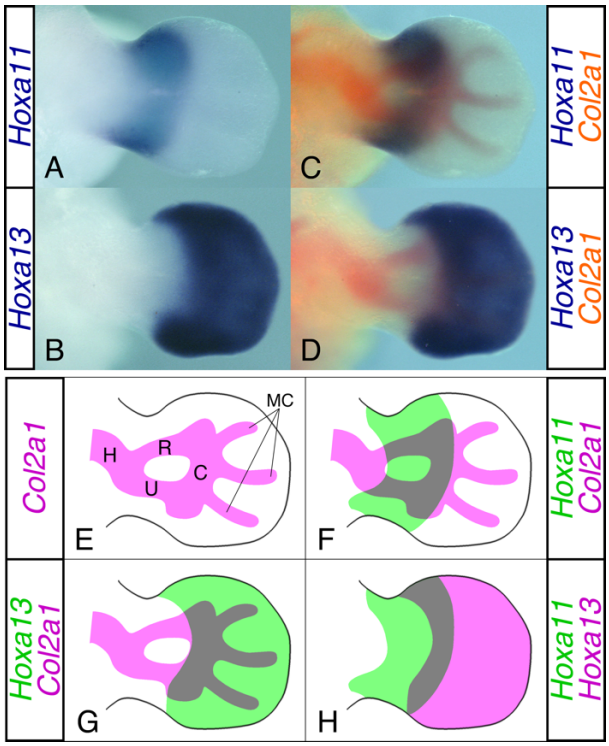

Fig. 1 Correlation between the *Hox* expression domain and cartilage in the E11.75 mouse forelimb bud. Dorsal view of *in situ* hybridizations for (A) *Hoxa11*and (B) *Hoxa13*. The cartilage pattern was visualized based on the *Col2a1* expression (red) in the same limb bud (C and D). (B) and (D) are presented as a digitally inverted (left-right) views of the original picture. (E) Illustration of the cartilage pattern shown in (C). H: humerus, R: radius, U: ulna, C: carpus, MC: metacarpus. (F) and (G) Representative drawings of (C) and (D), respectively. (H) Superimposed view of the *Hoxa11* and *Hoxa13* expression domains. Images redrawn based on relative location of each *Hox* expression domain to the cartilage pattern shown in (F) and(G). The left and right limb buds were isolated from a single embryo at E11.75 and were hybridized with DIG-labeled *Hoxa11* and fluorescein-labeled *Col2a1* probe mixture and DIG-labeled *Hoxa13* and fluorescein-labeled *Col2a1* probe mixture, respectively. *Hox* expression was detected using anti-DIG IgG-alkaline phosphatase (AP) with BM Purple as the substrate (blue). After inactivating AP activity, *Col2a1* expression was detected using anti-fluorescein IgG-AP with Fast Red as the substrate (red).

Figure 2

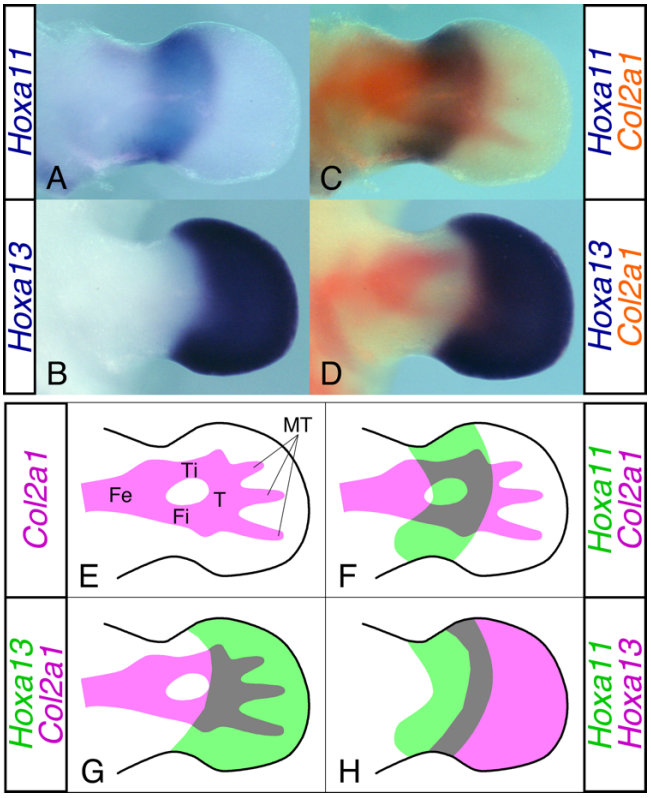

Fig. 2 Correlation between the *Hox* expression domain and cartilage in the E11.75 mouse hindlimb bud. Dorsal view of *in situ* hybridizations for (A) *Hoxa13* and (B) *Hoxa11*. The cartilage pattern was visualized based on *Col2a1* expression (red) in the same limb bud (C and D). (B) and (D) are presented as a digitally inverted (left-right) views of the original picture. (E) Illustration of the cartilage pattern shown in (C). Fe: femur, T: tibia, Fi: fibula, T: tarsus, MT: metatarsus. (F) and (G) Representative drawings of (C) and (D), respectively. (H) Superimposed view of *Hoxa11* and *Hoxa13* expression domains. Images redrawn based on the location of each *Hox* expression domain relative to the cartilage pattern shown in (F) and (G). The left and right limb bud were isolated from a single embryo at E11.75 and were hybridized with DIG-labeled *Hoxa11* and fluorescein-labeled *Col2a1* probe mixture, and DIG-labeled *Hoxa13* and fluorescein-labeled *Col2a1* probe mixture, respectively. *Hox* expression was detected using anti-DIG IgG-alkaline phosphatase (AP) with BM Purple as the substrate (blue). After inactivating AP activity, *Col2a1* expression was detected using anti-fluorescein IgG-AP with Fast Red as the substrate (red).

The HOXA11 and HOXA13 DNA binding regions overlap in the limb bud

To assess the zeugopodal and autopodal *Hox* target genes during the cartilage formation at E11.5 when metacarpal/metatarsal anlage just begins to protrude from carpal/tarsal anlage, ChIP-Seq analysis was carried out and the DNA regions associated with HOXA11 or HOXA13 proteins were identified. The number of independent HOXA11 and HOXA13 ChIP peaks were 2953 and 143,460, respectively (Table 1a). The number of HOXA11 peak is comparable to that of recently reported HOXC10 ChIP-Seq peak in the E11.5 limb bud (Jain et al. 2018). Fig. 3A-C and Fig. 4A-C show the integrative genome viewer (IGV) representation of HOXA11, HOXA13 and other homeodomain transcription factor binding sites in the representative gene loci.

In the *HoxA* cluster, HOXA13 binding regions were present in the intron of *Hoxa7* (arrow), the 3'UTR of *Hoxa9* (open arrowhead) and the intron of *Hoxa11* (arrowhead) (Fig. 3A). The *Hoxa11* intronic binding site is crucial for HOXA13-dependent repression of *Hoxa11* in the autopod (Kherdjemil et al. 2016). In contrast to the binding of both HOXA11 and HOXA13 to the *Hoxa7* and *Hoxa9* regions, only HOXA13 binding was observed in

the *Hoxa11* intron. This indicates different contributions of HOXA11 and HOXA13 to the control of *Hoxa11* expression.

As shown in the IGV for other representative gene loci (Fig. 3B, C and Fig. 4A-C), multiple HOX11/13 binding sites are present and many of the HOXA11 and HOXA13 binding sites overlap with each other. To further analyze this overlap, the accumulation of ChIP-Seq reads around the peak summit was determined. As shown in Fig. 5A, significant accumulation of the HOXA13 ChIP-Seq signal was found within 200 bp of the HOXA11 ChIP peak and *vice versa* (Fig. 5B). Regions that showed the summit of each peak located within 1 kb were selected. Of these colocalized sites, 75% of the ChIP-peak summits were located within 200 bp of each other (Fig. 5C). The results that the summits are in close proximity and that both HOXA11 and HOXA13 bind the same target sequence *in vitro* (Shen et al. 1997), suggest that HOX11 and HOXA13 binds the same target *in vivo*. Regions that exhibited directly overlapping peak spans were further selected and it was found that 2139 HOXA11 binding regions of their expression domain (distal zeugopod and proximal autopod) overlapped with the autopodal HOXA13 peak. These overlapping

peaks are 72% of the total HOXA11 peak (Table 1a) indicating that a considerable portion of the HOXA11 binding regions are common to the HOXA13 binding region. This common region was subsequently referred as the CHBRL (Common Hox binding region of the limb bud). Significant accumulation of both HOXA11 and HOXA13 ChIP-Seq reads was confirmed around the CHBRL (Fig.5D).

As shown in Fig. 5E, the CHBRL was located a long distance (50-500 kb) from the transcription start site (TSS) and most of the CHBRL was located within the intronic or intergenic region (Fig. 5F). HOXA13 binding in the E11.0 and E12.5 limb bud was also analyzed and it was found that a considerable portion of the CHBRL (E11.5) was common to both E11.0 (798/2139, 37%) and E12.5 (1618/2139, 76%) HOXA13 ChIP peaks (Table 1b).

Figure 3

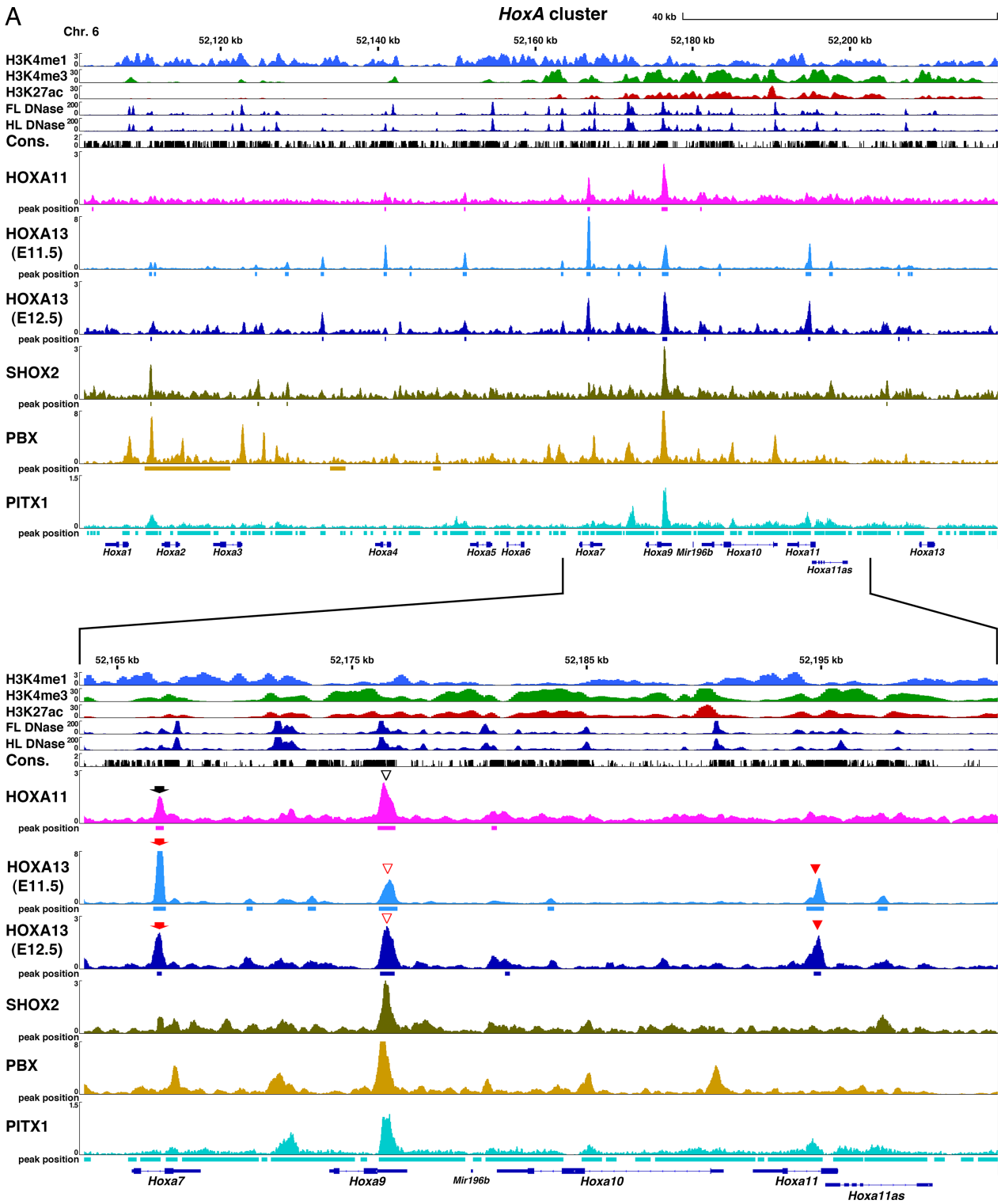
A
Chr. 6
HoxA cluster
40 kb
52,120 kb
52,140 kb
52,160 kb
52,180 kb
52,200 kb
H3K4me1
H3K4me3
H3K27ac
FL DNase
HL DNase
Cons.
HOXA11
peak position
HOXA13 (E11.5)
HOXA13 (E12.5)
SHOX2
PBX
PITX1
Hoxa1
Hoxa2
Hoxa3
Hoxa4
Hoxa5
Hoxa6
Hoxa7
Hoxa9
Mir196b
Hoxa10
Hoxa11
Hoxa13
Hoxa11as
52,165 kb
52,175 kb
52,185 kb
52,195 kb

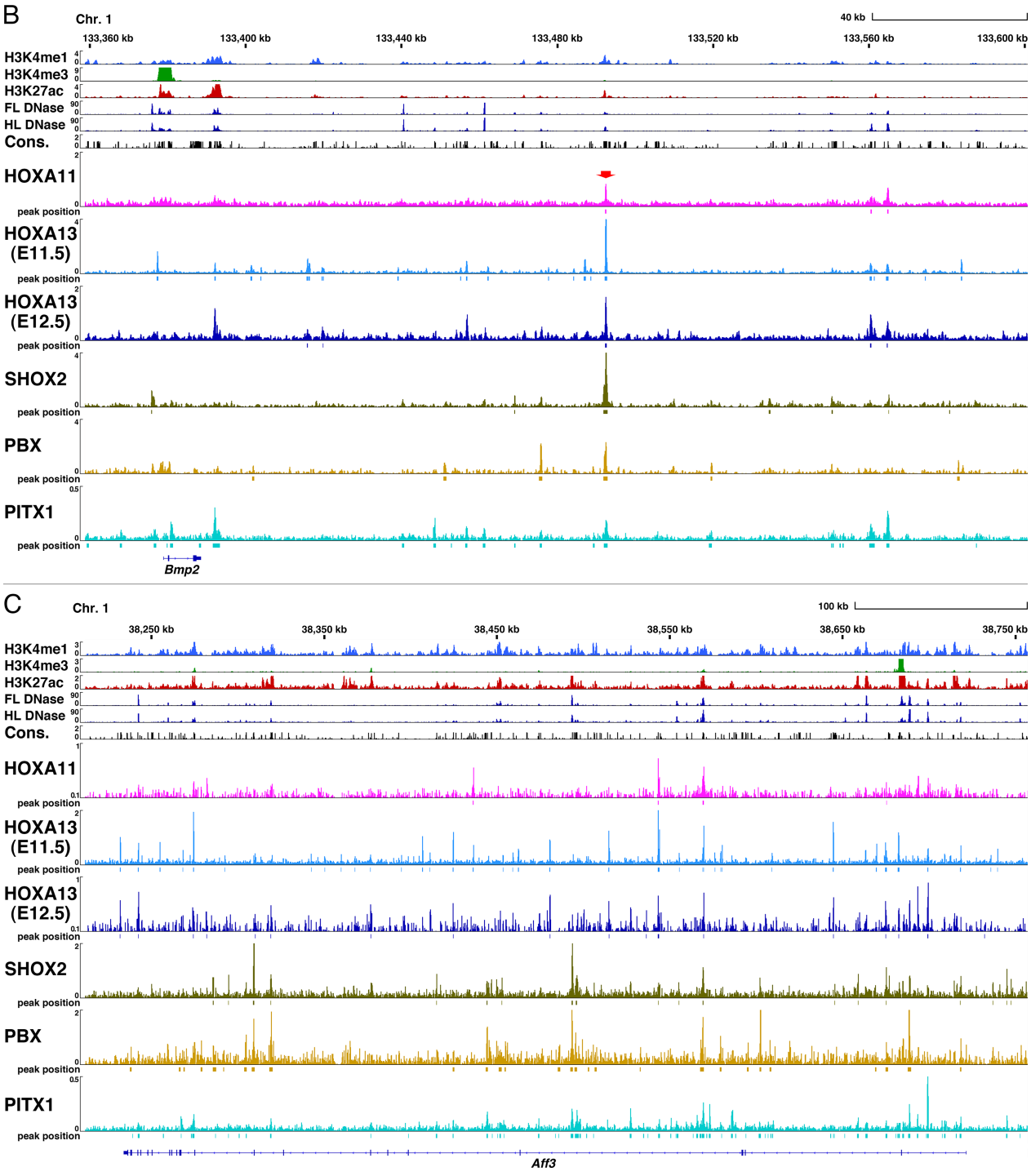
B
Chr. 1
40 kb
133,360 kb
133,400 kb
133,440 kb
133,480 kb
133,520 kb
133,560 kb
133,600 kb
H3K4me1
H3K4me3
H3K27ac
FL DNase
HL DNase
Cons.
HOXA11
peak position
HOXA13 (E11.5)
HOXA13 (E12.5)
SHOX2
PBX
PITX1
Bmp2
C
Chr. 1
100 kb
38,250 kb
38,350 kb
38,450 kb
38,550 kb
38,650 kb
38,750 kb
Aff3

Fig. 3 IGV view of HOX11/13 and homeodomain transcription factors in the limb bud.
(A) *HoxA* cluster, (B) *Bmp2*, (C) *Aff3*. The epigenetic state of each gene determined by enrichment of H3K4me1, H3K4me3 and H3K27ac in the limb buds and DNase I hypersensitivity sites in the E11.5 limb bud (FL DNase, HL DNase, FL: forelimb bud, HL: hindlimb bud) and sequence conservation among vertebrates (Phastcons [Vertebrate 30way]) presented as a bar graph. Data were obtained from public data bases as described in Table 6. ChIP-Seq data for HOXA11 and HOXA13 using E11.5 limb bud (HOXA11 and HOXA13(E11.5)) and E12.5 autopod (HOXA13(E12.5)) from this study are presented as a bar graph. The SHOX2 and PBX binding profiles in the E12.5 limb bud and the PITX1 binding profile in the E11.5 hindlimb bud were visualized by reanalysis of published data source presented in Table 6 using the same platform as for the HOX11/13 data. Numbers in the vertical axis indicate coverage values that were scaled by 1,000,000/total count. Squares beneath the peak indicate the region identified as transcription factor binding by MACS2 analysis. (A) Arrow: intron of *Hoxa7*, open arrowhead: 5' UTR of *Hoxa9*, arrowhead: intron of *Hoxa11*. (B) Arrow: the CHBRL deleted in *Bmp2cis*KO in Fig. 10.

Figure 4

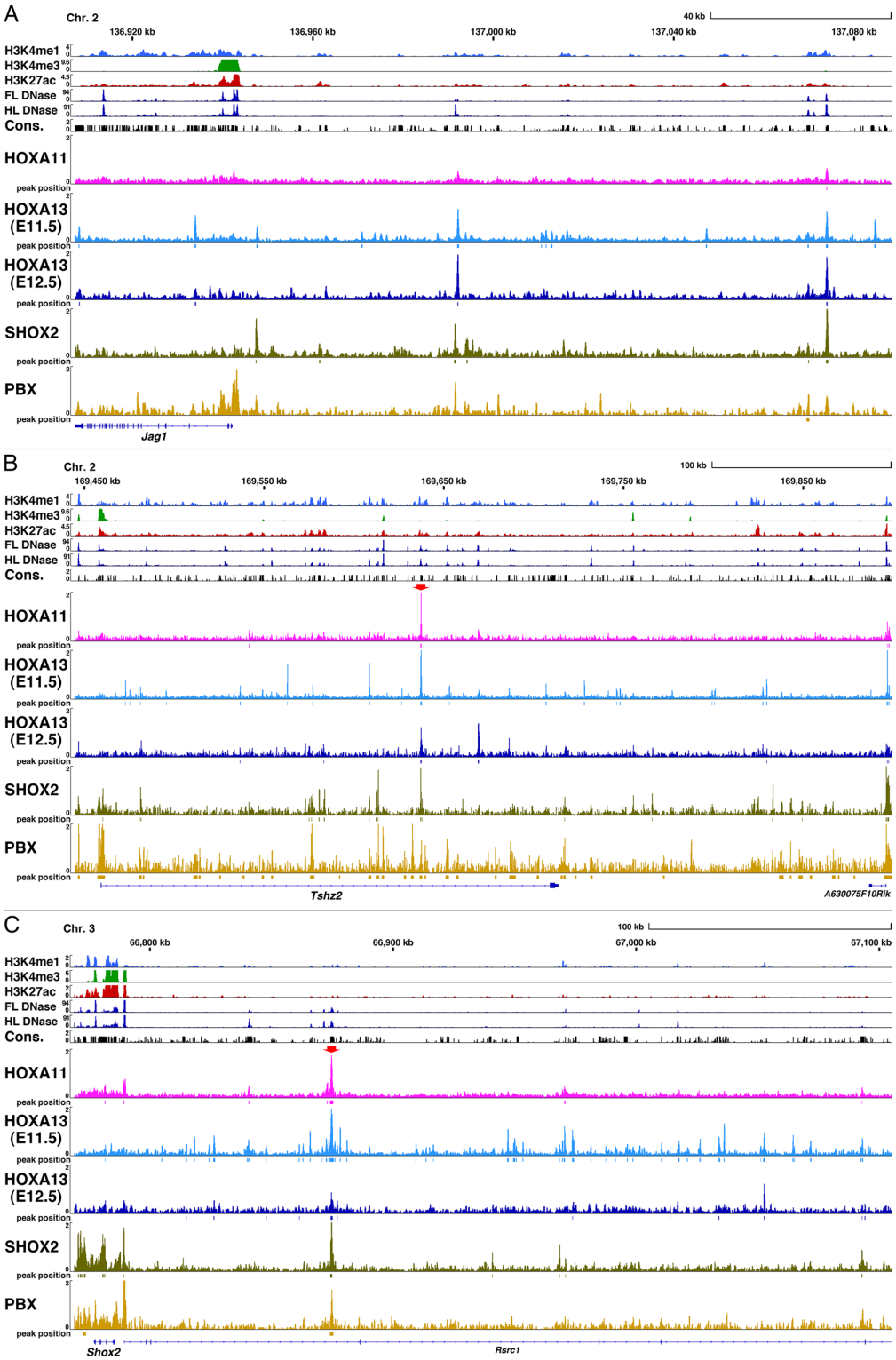
A
Chr. 2
40 kb
136,920 kb
136,960 kb
137,000 kb
137,040 kb
137,080 kb
H3K4me1
H3K4me3
H3K27ac
FL DNase
HL DNase
Cons.
HOXA11
peak position
HOXA13 (E11.5)
peak position
HOXA13 (E12.5)
peak position
SHOX2
peak position
PBX
peak position
Jag1
B
Chr. 2
100 kb
169,450 kb
169,550 kb
169,650 kb
169,750 kb
169,850 kb
H3K4me1
H3K4me3
H3K27ac
FL DNase
HL DNase
Cons.
HOXA11
peak position
HOXA13 (E11.5)
peak position
HOXA13 (E12.5)
peak position
SHOX2
peak position
PBX
peak position
Tshz2
A630075F10Rik
C
Chr. 3
100 kb
66,800 kb
66,900 kb
67,000 kb
67,100 kb
H3K4me1
H3K4me3
H3K27ac
FL DNase
HL DNase
Cons.
HOXA11
peak position
HOXA13 (E11.5)
peak position
HOXA13 (E12.5)
peak position
SHOX2
peak position
PBX
peak position
Shox2
Rsrc1

Fig. 4 IGV view of HOX11/13 and homeodomain transcription factors in the limb bud.

(A) *Jag1*, (B) *Tshz2*, (C) *Shox2*. The epigenetic state of each gene was determined based on the enrichment of H3K4me1, H3K4me3 and H3K27ac and the DNase I hypersensitivity sites of the E11.5 limb bud, (FL DNase, HL DNase, FL: forelimb bud, HL: hindlimb bud) and sequence conservation among vertebrates (phyloP[Vertebrate 30 way]) are presented as a bar graph. Data were obtained from public databases as described in Table S6. ChIP-Seq data for HOXA11 and HOXA13 using the E11.5 limb bud (HOXA11 and HOXA13(E11.5)) and E12.5 autopod (HOXA13(E12.5)) from this study are presented as a bar graph. The SHOX2 and PBX binding profiles of the E12.5 limb bud was visualized by reanalysis of published data GSE81897 (NCBI) using the same platform as for the *Hox* data. Numbers in the vertical axis indicate coverage values that were scaled by 1,000,000/total count. Squares beneath the peak indicate the region identified as transcription factor binding by MACS2 analysis. (B) Arrow: the CHBRL deleted in *Tshz2cis*KO in Fig. 10. (C) Arrow: the region carries limb specific enhancer activity.

Figure 5

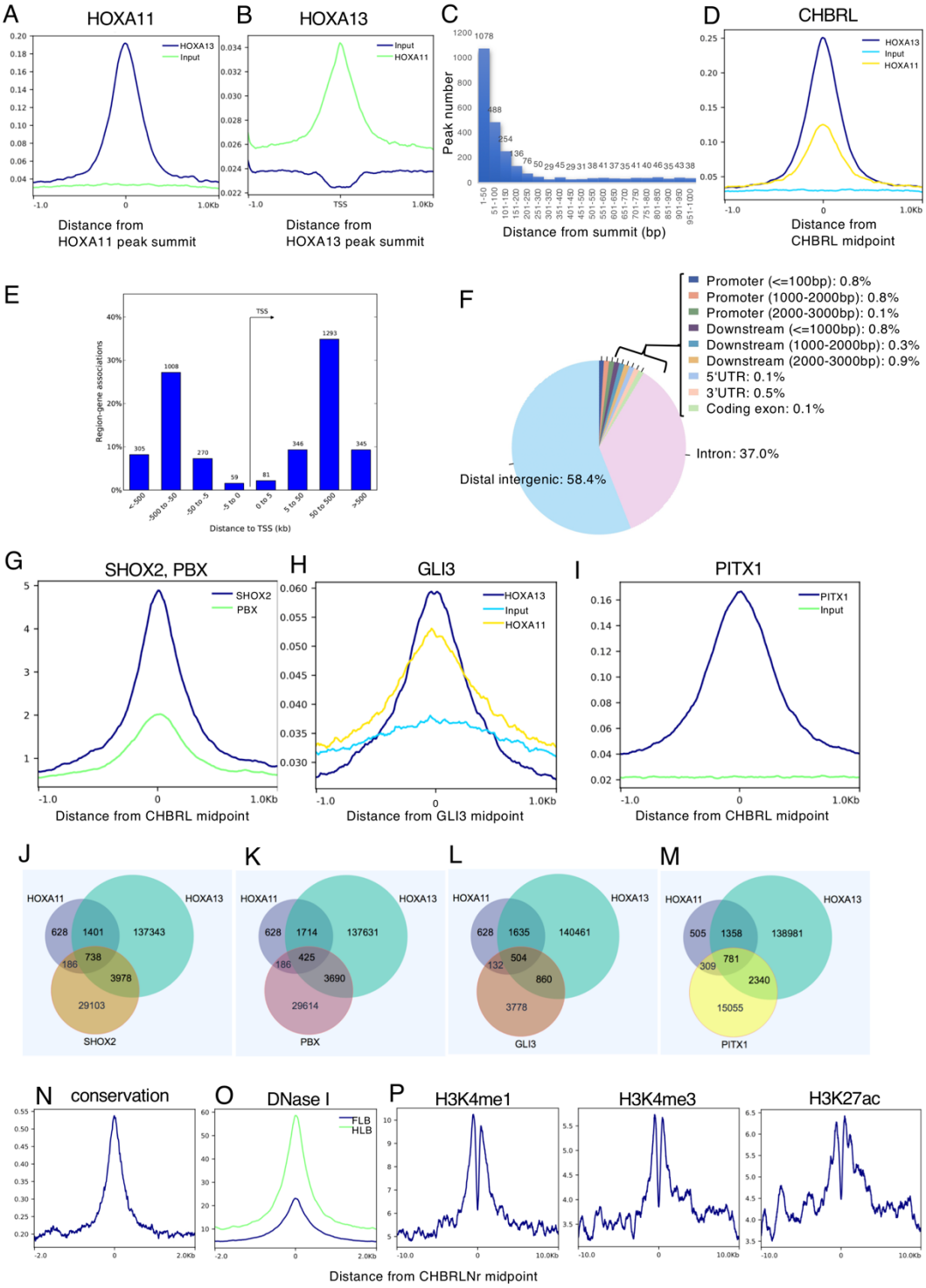
A
HOXA11
HOXA13
Input
Distance from
HOXA11 peak summit
B
HOXA13
Input
HOXA11
TSS
Distance from
HOXA13 peak summit
C
Peak number
Distance from summit (bp)
D
CHBRL
HOXA13
Input
HOXA11
Distance from
CHBRL midpoint
E
Region-gene associations
Distance to TSS (kb)
F
Promoter (<=100bp): 0.8%
Promoter (1000-2000bp): 0.8%
Promoter (2000-3000bp): 0.1%
Downstream (<=1000bp): 0.8%
Downstream (1000-2000bp): 0.3%
Downstream (2000-3000bp): 0.9%
5'UTR: 0.1%
3'UTR: 0.5%
Coding exon: 0.1%
Intron: 37.0%
Distal intergenic: 58.4%
G
SHOX2, PBX
SHOX2
PBX
Distance from CHBRL midpoint
H
GLI3
HOXA13
Input
HOXA11
Distance from GLI3 midpoint
I
PITX1
PITX1
Input
Distance from CHBRL midpoint
J
HOXA11
HOXA13
628
1401
137343
738
186
3978
29103
SHOX2
K
HOXA11
HOXA13
628
1714
137631
425
186
3690
29614
PBX
L
HOXA11
HOXA13
628
1635
140461
504
132
860
3778
GLI3
M
HOXA11
HOXA13
505
1358
138981
781
309
2340
15055
PITX1
N
conservation
O
DNase I
FLB
HLB
P
H3K4me1
H3K4me3
H3K27ac
Distance from CHBRLNr midpoint

Fig. 5 Profile of the limb HOX11/13 DNA binding region.

Condensed profiles of ChIP-Seq signals of (A) HOXA13 for HOXA11 peak summits or (B) HOXA11 for HOXA13 peak summit. (C) Distribution plot for distances between HOXA11 and HOXA13 peak summits located within 1 kb each other. (D) Condensed profiles of ChIP-Seq signals for the CHBRL. (E) The majority of the CHBRL peaks are located a great distance from their nearest transcription starting site (TSS). (F) The majority of CHBRL peaks are located at the intronic or distal intergenic region of the chromosome. (G) Aggregate plots of SHOX2 and PBX binding signals in the embryonic limb at E11.5 centered around the CHBRL. (H) Aggregate plots of HOXA11and HOXA13 binding signals in the embryonic limb at E11.5 centered around the summits of Gli3 binding region. (I) Aggregate plots of PITX1 binding signals in the embryonic limb at E11.5 around centered around the CHBRL. The number of the overlapping ChIP-Seq peaks of HOXA11 and HOXA13 with (J) SHOX2, (K) PBX, (L) GLI3 and (M) PITX1. (N) Aggregate plots based on average phastcons [60way.phastCons] across vertebrates indicate that the majority of the CHBRLNrs are highly conserved. (O) Aggregate plots on DNase I hyper-sensitive sites in embryonic fore-(FLB) and hindlimb (HLB) at E11.5 around the center of the CHBRLNr. (P) Aggregate plots of H3Kme1, H3K4me3 and H3K27ac binding signals in the embryonic limb at E11.5 around the center of the CHBRLNr. Data source was presented in Table 6. Numbers in the vertical axis of A, B, D, G-I and N-P indicate average signal per base (see Materials and Methods).

The CHBRL overlaps with limb SHOX2, PBX, GLI3 or PITX1 binding regions

The homeodomain transcription factors SHOX2 and PBX are also expressed in the limb bud mesenchyme and have important roles in limb cartilage development (Selleri et al. 2001;Cobb et al. 2006). In addition, as shown in Fig. 3A-C and Fig. 4A-C, some HOX binding regions displayed overlap with the SHOX2 and/or PBX binding peaks suggesting that they may share common targets with HOX11/13. Thus, the overlap between the HOX11/13 binding region and the reported SHOX2, or PBX binding region (Ye et al. 2016)was analyzed. Reported ChIP-Seq reads for both SHOX2 and PBX significantly accumulated around the CHBRL (Fig. 5G). As shown in Fig.5 J, K, Table 1b, and Fig. 4, a substantial number of the HOX11/13 binding regions overlapped with the SHOX2 and/or PBX binding regions, although they exhibited variation in their combinations. The HOX11/13 binding region of *Bmp2* (Fig. 3B), *Tshz2*, *Jag1* and *Shox2* (Fig. 4A-C, respectively) overlapped with the SHOX2 binding regions; however, the major HOX11/13 binding region in the *HoxA* cluster did not show overlap with SHOX2 binding (Fig. 3A). In contrast, some of the HOX11/13 binding regions in *Aff3* overlapped with the SHOX2

binding regions, although other HOX11/13 binding regions in *Aff3* did not show SHOX2 binding (Fig. 3C). HOX and SHOX2 share a common binding core sequence *in vitro* suggesting they may also share common binding sites *in vivo* or they bind to different sites in the CHBRLs, as multiple HOX11/13 binding sites are demonstrated in Fig. 7-9. On the other hands, these results also indicate variation in the overall binding repertoire of each homeodomain transcription factor.

The transcription factor GLI3 also has a crucial role in limb morphogenesis as the target of the *Shh* signaling pathway (Buscher et al. 1997). Because GLI3 cooperates with 5' *Hox* genes in cartilage pattern formation of the limb (Chen et al. 2004, Zakany et al. 2007), the CHBRL was compared with the GLI3 binding regions in the limb bud (Vokes et al. 2008). The ChIP-Seq reads showed modest accumulation around the GLI3 ChIP peak (Fig. 5H). Interestingly, 24% (504/2139; Fig. 5L and Table 1b) of the CHBRL overlapped with the GLI3 binding region suggesting that functional cooperation may occur directly through co-occupation of HOX11/13 and GLI3 in the regulatory element of their target genes (Table 2). The paired-type homeodomain transcription factor PITX1 is also involved

in limb cartilage pattern formation (Szeto et al. 1999). As shown in Fig.3A-C, many PITX1 ChIP-Seq peaks overlapped with HOX11/13 peaks and PITX1 ChIP-Seq reads significantly accumulated around the CHBRL (Fig. 5I). The 59% of the CHBRL was found to overlap with the PITX1 binding region (Nemec et al. 2017) (Fig. 3M and Table 1b).

The CHBRL correlates with limb-specific chromatin epigenetic states

The profile of the CHBRL was further analyzed in relation to the epigenetic state of the limb bud chromatin. After eliminating the regions containing repetitive sequences from the CHBRL pool, most of the remaining regions, the CHBRLNr (CHBRL with no repetitive sequences, 1518/2139, 71%; Table 1b) exhibited significant overlap with conserved sequence shared among vertebrates (1506/1518, 99%; Fig. 5N); a representative comparison is shown in Fig. 7 and Fig. 9I-L. The DNase I hypersensitive region of the limb bud was significantly localized around the CHBRLNr (Fig. 5O). Of the CHBRLNr, 73% (1107/1518; Table 1b) showed overlap with the DNase I hypersensitivity region in the E11.5 limb bud (Yue et al. 2014).

To further define the chromatin epigenetic state around the CHBRLNr, the histone modification profiles was evaluated. As shown in Fig. 5P, H3K4me1, H3K4me3 and H3K27ac were enriched around the CHBRL. Representative overlapping of the HOXA11 or HOXA13 peaks with the modified histon region is also shown in Fig. 3A-C and Fig. 4A-C. Interestingly, 70% (1063/1518; Table 1b) of the conserved CHBRLNr overlapped with the region enriched for H3K27ac suggesting that a significant part of the CHBRLNr participates in potential enhancer function in the limb bud. A deep trough in the middle of the histone modification peaks shown in Fig. 5P suggest that CHBRLNr corresponds to a nucleosome-free (depleted) region. This is supported by that DNase I hyper-sensitive sites are enriched around CHBRLNr shown Fig. 5O. By matching with the limb enhancer regions provided by the VISTA program (Visel et al. 2007), 57 regions out of 334 regions in the VISTA limb enhancer were found to correspond with the CHBRLNr (Table 1b) including the *Shox2* enhancer (Rosin et al. 2013;Osterwalder et al. 2018) located in the intron of the neighboring gene *Rsrc1* (Fig. 4C arrow). In addition, the CHBRLNr shown in Fig. 3B (arrow) was also included in the region possessing the distal limb bud enhancer

of *Bmp2* (Dathe et al. 2009). These results indicate that a particular member of the CHBRLNr actually possesses the limb-specific enhancer function.

Multiple HBSs were enriched in the HOX11/13 ChIP fragments

ABD-B type HOX proteins bind to both the TTAT/C and TAAT/C motifs (HOX binding sequence: HBS) *in vitro* (Shen et al. 1997). Thus, the enrichment of these sequences in the HOXA11 and HOXA13 ChIP fragment and the CHBRLNr was analyzed. As shown in Fig. 6, the sequences containing TTAT or TAAT were highly enriched in the HOX11/13 ChIP fragment indicating that HOX11/13 proteins directly bind to the majority of the ChIP fragment *in vivo*. Interestingly, as shown in representative results in Fig. 7B, C and Fig. 9I-L, evolutionarily conserved multiple HBSs were found in most of the ChIP DNA.

Figure 6

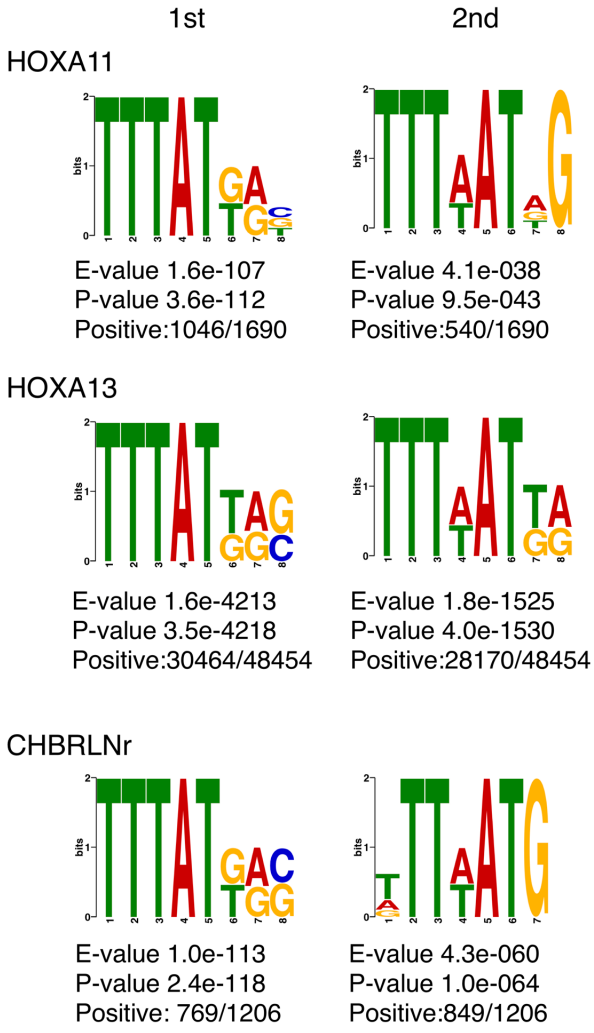

Fig. 6 The Abd-B HOX binding motif was enriched in the HOXA11 and HOXA13 ChIP recovered DNA from the limb bud. The top two motifs of HOXA11 or HOXA13 ChIP DNA and the DNA fragment exhibiting common binding of CHBRLNr are shown. Results of DREME analysis are presented.

HOX11/13 protein directly binds to the evolutionarily conserved HBSs in the ChIP DNA

As described above, the nucleotide sequences encoded by most HOX11/13 ChIP fragments showed evolutionary conservation. Among them, the HOX protein binding consensus core sequence, HBS, exhibited a high level of conservation (Fig. 7B, C and Fig. 9I-L). Then, direct HOX11/13 protein binding to typical CHBRLs was analyzed *in vitro* by EMSA.

One of the CHBRLs in the *Rsrc1* intron (Fig. 4C, arrow), m741 (VISTA), carries the limb-mesenchyme specific enhancer function of the neighboring *Shox2* gene (Rosin et al. 2013;Osterwalder et al. 2018). m741 contains highly conserved multiple HBSs, which are concentrated in the two sub-regions, 741b and 741c (Fig. 7A). As shown in Fig. 8A, B and Fig. 9A, B, in the presence of HOXA13HOMEODOMAIN (HD) both the 741b and 741c probes showed multiple shift bands in a HOXA13HD protein dose-dependent manner indicating that HOXA13 has multiple binding sites in the probe. These shift bands were competed by oligonucleotides containing HBS1 (TTAT) or HBS2 (TAAT) but

not competed by oligonucleotides containing mutated HBS (Fig. 8B and Fig. 9B). HOXA11HD also showed the same binding profile as HOXA13HD to the 741b and 741c probes (Fig. 8C, D and Fig. 9C, D). These results indicate that HOX11/13 protein directly binds to the HBSs in the 741b and 741c. The CHBRLs of *Bmp2*, *Jag1* and *Tshz2*, in addition to one of the *Aff3* CHBRLs, also contain multiple HBSs (Fig. 9I-L). Both HOXA11HD and HOXA13HD bound these fragments in an HBS-dependent manner indicating that HOX11/13 proteins directly bind to the conserved HBSs in the CHBRL (Fig. 8E-H and Fig. 9E-H).

Figure 7

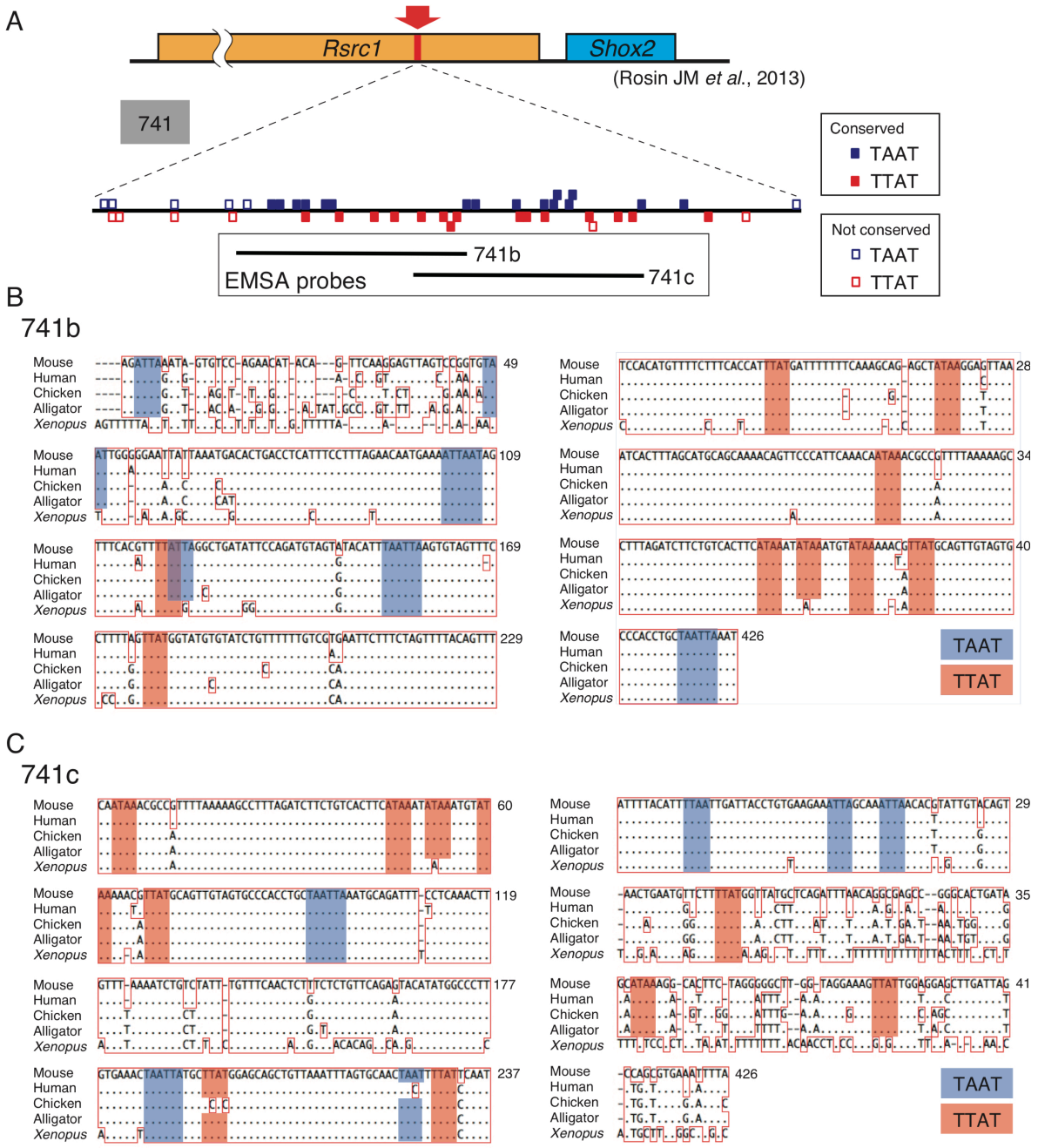

Fig. 7 The sequence of the *Shox2* enhancer is conserved among tetrapods and contains highly conserved multiple HBSs. One of the *Shox2* limb bud enhancers is located in the intron of the neighboring gene *Rsrc1* (VISTAm741, (Rosin et al. 2013)). The location and sequence of the EMSA probes, 741b and 741c, are shown. Conserved HBSs are clustered in the sub-regions 741b and 741c.

Figure 8

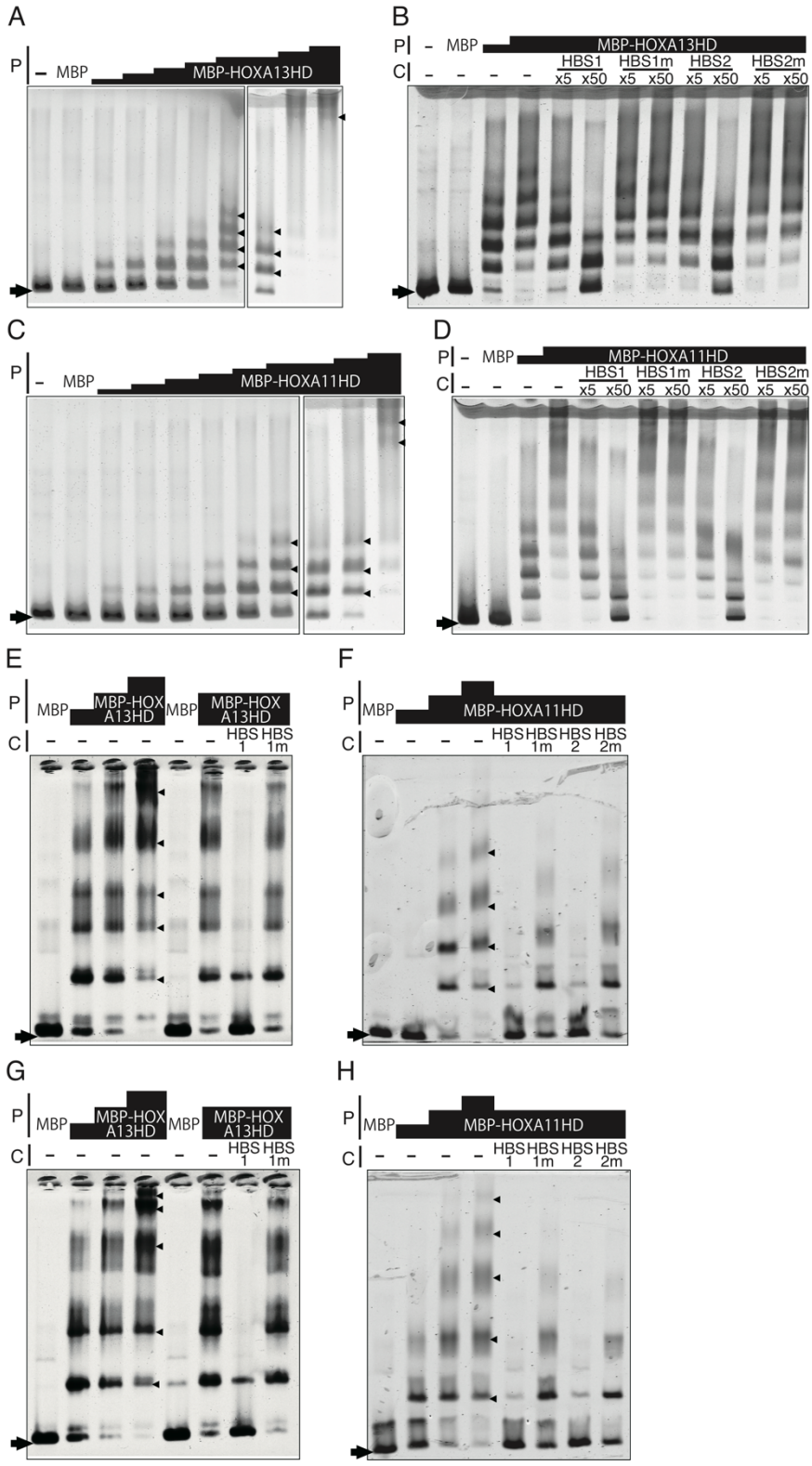
A
P
–
MBP
MBP-HOXA13HD
B
P
–
MBP
MBP-HOXA13HD
C
–
–
–
–
HBS1
x5
x50
HBS1m
x5
x50
HBS2
x5
x50
HBS2m
x5
x50
C
P
–
MBP
MBP-HOXA11HD
D
P
–
MBP
MBP-HOXA11HD
C
–
–
–
–
HBS1
x5
x50
HBS1m
x5
x50
HBS2
x5
x50
HBS2m
x5
x50
E
P
MBP
MBP-HOX A13HD
MBP
MBP-HOX A13HD
C
–
–
–
–
–
–
HBS 1
HBS 1m
F
P
MBP
MBP-HOXA11HD
C
–
–
–
–
HBS 1
HBS 1m
HBS 2
HBS 2m
G
P
MBP
MBP-HOX A13HD
MBP
MBP-HOX A13HD
C
–
–
–
–
–
–
HBS 1
HBS 1m
H
P
MBP
MBP-HOXA11HD
C
–
–
–
–
HBS 1
HBS 1m
HBS 2
HBS 2m

Fig. 8 HOXA11 and HOXA13 bind to multiple HBSs in the CHBRL *in vitro*.

EMSAs using 741b, a part of the *Shox2* CHBRL/m741 enhancer (VISTA), as a probe. (A) Multiple shift bands emerged in a HOX protein dose-responsive manner; (-): no protein; MBP: 153 ng of MBP was added to the reaction. The amount of MBP-HOXA13HD used was 7.6, 15.2, 42, 85, 152, 152, 306 and 612 ng. (B) Band shift was competed by HBS-containing oligonucleotides HBS1 (TTAT) and HBS2 (TAAT) but not by their mutant forms (T to G and A to C). 153 ng of MBP and 128 or 255 ng of MBP-HOXA13HD were used. 5-fold or 50-fold excess molar unlabeled competitor was added to the reaction. (C) Multiple shift bands emerged in a HOX11/13 protein dose-responsive manner; (-): no protein, MBP; 153 ng of MBP was added to the reaction. The amount of MBP-HOXA11HD added was 1.4, 2.8, 5.7, 11.4, 28, 57, 57, 114, 228 ng. (D) Band shift was competed by HBS containing oligonucleotides HBS1 (TTAT) and HBS2 (TAAT) but not by their mutant forms (T to G and A to C). 153 ng of MBP and 95 or 189 ng of MBP-HOXA11HD were used. 5-fold or 50-fold molar excess unlabeled competitor was added to the reaction. (E-H) Multiple shift bands emerged in the HOX11/13 protein in a dose-dependent manner and were specifically competed by HBS-containing oligonucleotides. (E, G) MBP-HOXA13HD and (F, H) MBP-HOXA11HD. (E) and (F) *Aff3* probe, (G) and (H) *Bmp2* probe. The sequence of the probe and conserved HBS are shown in Fig. 9 I and J. Arrowhead and arrow indicate the shift band and free probe, respectively. P: protein, C: competitor.

Figure 9

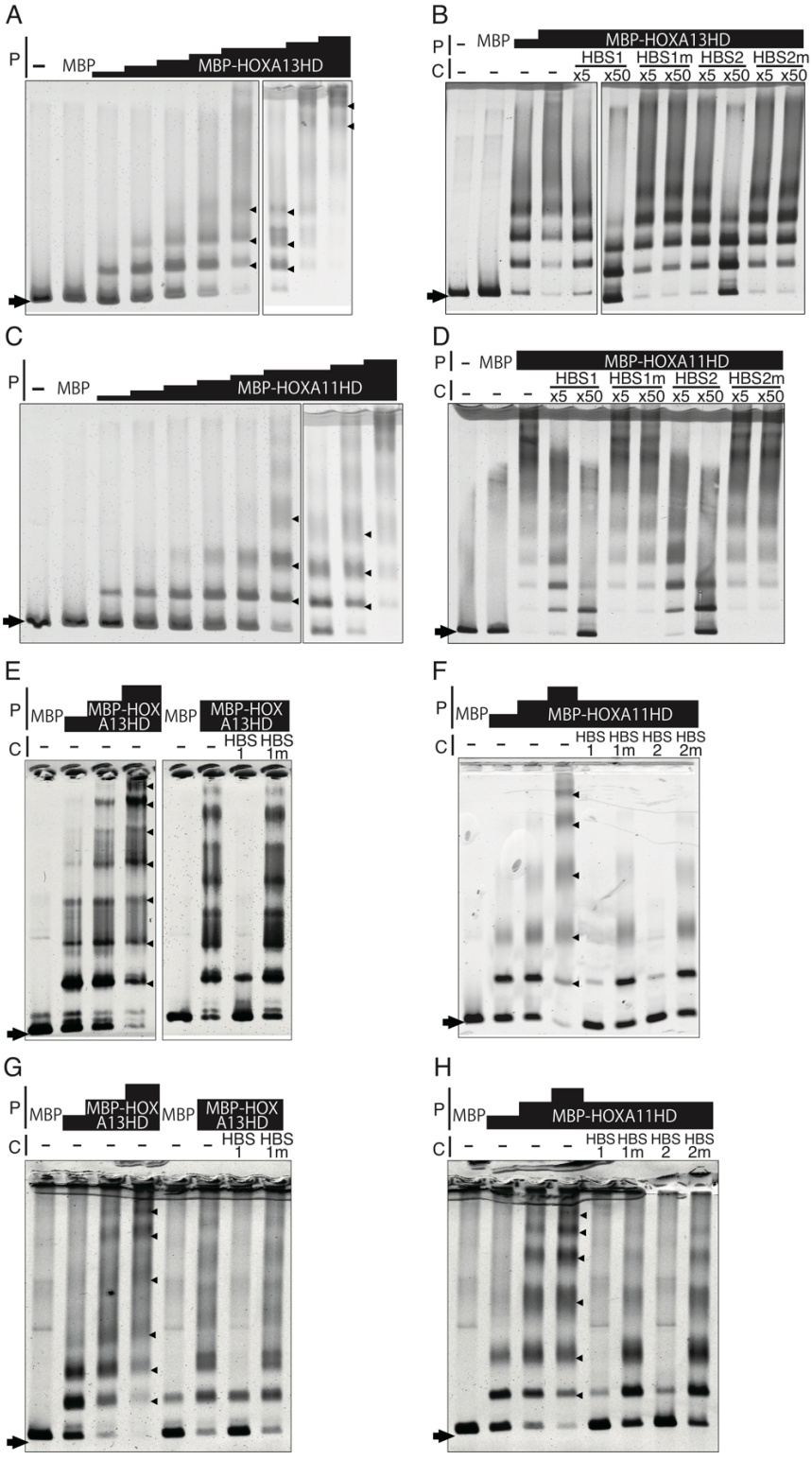
A
P
MBP
MBP-HOXA13HD
B
P
C
MBP
MBP-HOXA13HD
HBS1 HBS1m HBS2 HBS2m
x5 x50 x5 x50 x5 x50 x5 x50
C
P
MBP
MBP-HOXA11HD
D
P
C
MBP
MBP-HOXA11HD
HBS1 HBS1m HBS2 HBS2m
x5 x50 x5 x50 x5 x50 x5 x50
E
P
MBP
MBP-HOX A13HD
MBP
MBP-HOX A13HD
C
HBS 1
HBS 1m
F
P
MBP
MBP-HOXA11HD
C
HBS 1
HBS 1m
HBS 2
HBS 2m
G
P
MBP
MBP-HOX A13HD
MBP
MBP-HOX A13HD
C
HBS 1
HBS 1m
H
P
MBP
MBP-HOXA11HD
C
HBS 1
HBS 1m
HBS 2
HBS 2m

Fig. 9 HOXA11 and HOXA13 bind to multiple HBSs in the CHBRL *in vitro*.

EMSAs using 741c, a part of the *Shox2* CHBRL/m741 enhancer (VISTA), as a probe. (A) Multiple shift bands emerged in the HOX11/13 protein in a dose responsive manner. (-): no protein; MBP: 153 ng of MBP was added to the reaction. The amount of MBP-HOXA13HD used was 7.6, 15.2, 42, 85, 152, 152, 306 and 612 ng. (B) Band shift was competed by the HBS containing oligonucleotides HBS1(TTAT) and HBS2 (TAAT) but not by their mutant forms (T to G and A to C). 153 ng of MBP and 128 or 255 ng of MBP-HOXA13HD were used. 5-fold or 50-fold molar excess unlabeled competitor was added to the reaction. (C) Multiple shift bands emerged in the HOX11/13 protein in a dose responsive manner. (-): no protein; MBP: 153 ng of MBP was added to the reaction. The amount of MBP-HOXA11HD added was 1.4, 2.8, 5.7, 11.4, 28, 57, 57, 114, 228 ng. (D) Band shift was competed by the HBS-containing oligonucleotides HBS1 (TTAT) and HBS2 (TAAT) but not by their mutant form (T to G and A to C). 153 ng of MBP and 95 or 189 ng of MBP-HOXA11HD were used. 5-fold or 50-fold excess molar unlabeled competitor was added to the reaction. (E-H) Multiple shift bands emerged in the HOX11/13 protein in a dose dependent manner and were specifically competed by HBS-containing oligonucleotides. (E, G) MBP-HOXA13HD and (F, H) MBP-HOXA11HD. (E) and (F) *Jag1* probe, (G) and (H) *Tshz2* probe. The arrowhead indicates the shift band. The sequence of the CHBRL of (I) *Aff3*, (J) *Bmp2*, (K) *Jag1* and (L) *Tshz2.* The sequence used for the EMSA probe is indicated by a black bold overline. Multiple HBSs (TTAT/C, TAAT/C: square) are conserved among the amniotes. The arrowhead and arrow indicate the shift band and free probe, respectively. P: protein, C: competitor.

Chromosomal CHBRLs have limb-specific enhancer activity

It was next examined if the chromosomal CHBRLs are responsible for regulating neighboring gene expression in the limb bud. Considering that multiple enhancers have redundant function (Osterwalder et al. 2018), *Bmp2* and *Tshz2* were selected as a representative system. Both genes have one or two CHBRLs, so the most prominent CHBRLs was deleted using CRISPR/Cas9 system (*cis*KO). *Bmp2cis*KO mice was generated by deleting 1623 bp-containing CHBRL located about 100 kb downstream of the *Bmp2* coding region (Fig. 3B, arrow) and *Tshz2cis*KO mice by targeting a 1242 bp chromosomal region in the intron (Fig. 4B, arrow). As shown in Fig. 10A-F, in the *Bmp2CHBRL*$^{-/-}$ embryos, *Bmp2* expression in the distal mesenchyme was considerably reduced in the forelimb bud and barely detectable in the hindlimb bud. In the *Tshz2CHBRL*$^{-/-}$ embryos, *Tshz2* expression in the first interdigital region was slightly weakened in the forelimb bud and undetectable in the hindlimb bud (Fig. 10G-N, arrowheads and black arrows). In addition, weak expression in the anterior autopod was undetectable in both the forelimb and hindlimb buds of the *Tshz2CHBRL*$^{-/-}$ embryos

(Fig.10G, H, J-L and N, yellow arrows). These results indicate that the chromosomal CHBRLs possess the limb mesenchyme enhancer function in the *Hox* expressing domain.

Figure 10

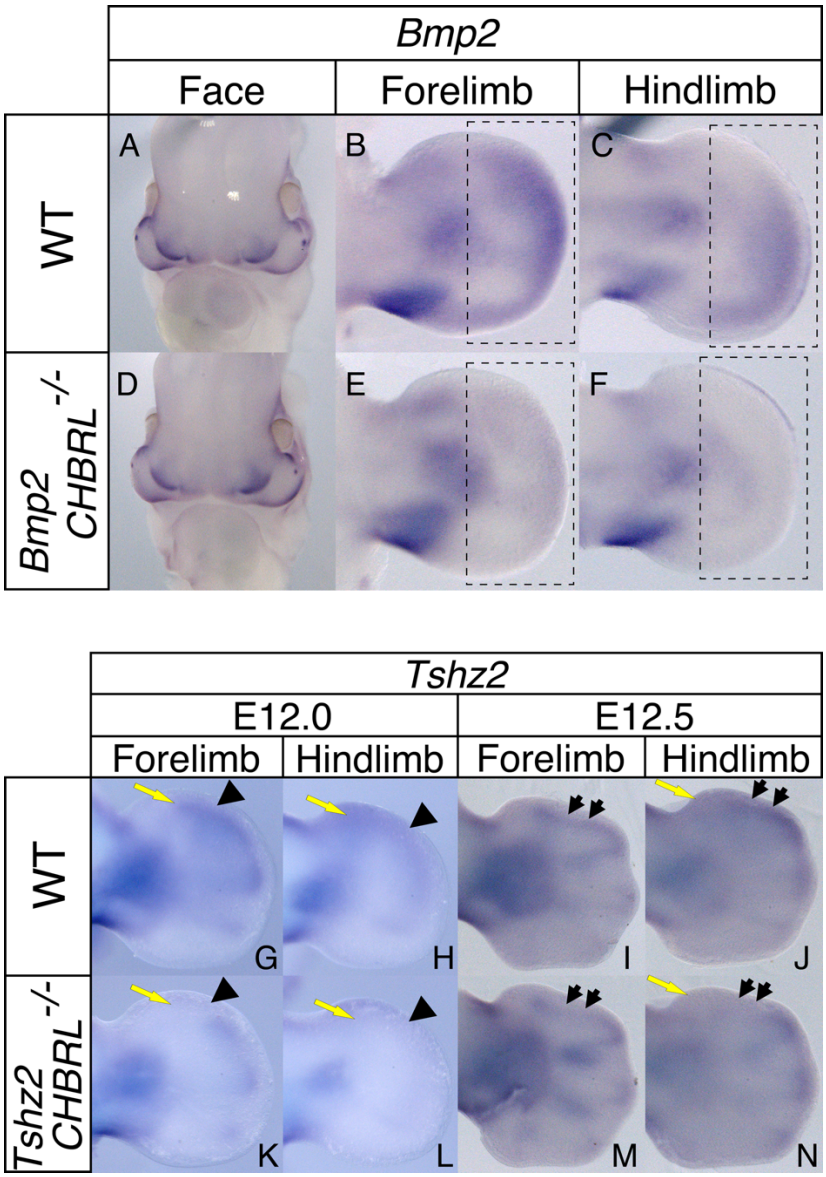

Fig. 10 CHBRLs of *Bmp2* and *Tshz2* have limb bud-specific enhancer function. Expression pattern of *Bmp2* in (A-C) wild-type and (D-F) *Bmp2CHBRL*$^{-/-}$ embryos. Facial *Bmp2* expression was not altered in the same (A and D) *Bmp2CHBRL*$^{-/-}$ embryos. The dotted squares indicate the region exhibiting reduced *Bmp2* expression in *Bmp2CHBRL*$^{-/-}$ embryos (compare B and E, C and F). Expression pattern of *Tshz2* in (G-J) wild-type and (K-N) *Tshz2CHBRL*$^{-/-}$ embryos. The arrowhead and arrow indicate the regions exhibiting reduced *Tshz2* expression in *Tshz2CHBRL*$^{-/-}$ embryos.

Genes neighboring the CHBRLNr show altered expression in *Hox11-13* mutant limbs

1556 genes neighboring the CHBRLNr (a11a13 genes, Table 2) were identified. Among these, genes related to skeletal development, limb development or cartilage morphology were enriched (Fig. 11A). Interestingly, genes related to skeletal development were also enriched in the gene groups whose CHBRLNr overlapped with the SHOX2, PBX1, PITX1 and GLI3 binding regions (Table 2, Fig. 11B-E). It was also found that most of the genes containing or neighboring the CHBRLNr belong to the same topologically associating domain (TAD) as the CHBRLNr (1232 /1556 genes, 79%; Table 2 and Table 4) indicating that these CHBRLNrs are involved in regulating the expression of flanking genes (Long et al. 2016). To verify these as the *Hox* target genes, the limb bud expression profile in wild-type and *Hox13* deleted embryos was analyzed.

Figure 11

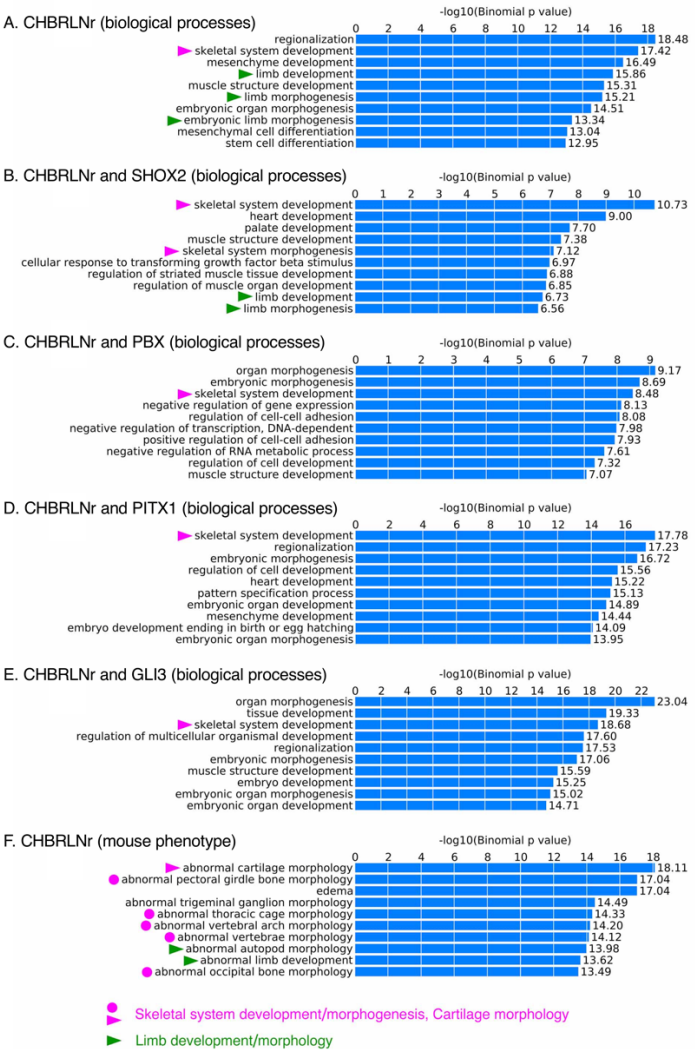

Fig. 11 Genes related to skeletal development are enriched in the gene pool containing the HOX and SHOX2/PBX/PITX1/GLI3 common region. (A) Gene ontology of the biological processes of the CHBRLNr genes, (B) genes neighboring the peak shared with CHBRLNr and SHOX2, (C) genes neighboring the peak shared with CHBRLNr and PBX, (D) genes neighboring the peak shared with CHBRLNr and PITX1, (E) genes neighboring the peak shared with CHBRLNr and GLI3 are shown. (F) Gene ontology of the mouse phenotype of the CHBRLNr genes. Data were obtained by GREAT analysis of the bed file in Table 2.

Hoxa13 and *Hoxd13* show overlapping expression in the autopodal mesenchyme and cooperatively function in autopodal cartilage pattern formation (Yokouchi et al. 1991;Fromental-Ramain et al. 1996). *Hoxd11* and *Hoxd12* are also expressed in the autopodal mesenchyme and cooperate in autopodal cartilage pattern formation in a gene dosage-dependent manner together with *Hoxa13* and *Hoxd13*. Specifically, homozygote with simultaneous deletion of *Hoxd11,12,13* (*HoxD*$^{del(11\text{-}13)}$) exhibited more severe adult cartilage phenotypes than *Hoxd13* KO homozygotes (Zakany et al. 1997). To increase the sensitivity in analyzing *Hox* function, *HoxD*$^{del(11\text{-}13)}$ and *Hoxa13*KO mice in this study were combined (hereinafter *Hoxa13*$^{-/-}$; *HoxD*$^{del(11\text{-}13)/del(11\text{-}13)}$ is abbreviated to as *Hox13*dKO).

Figure 12

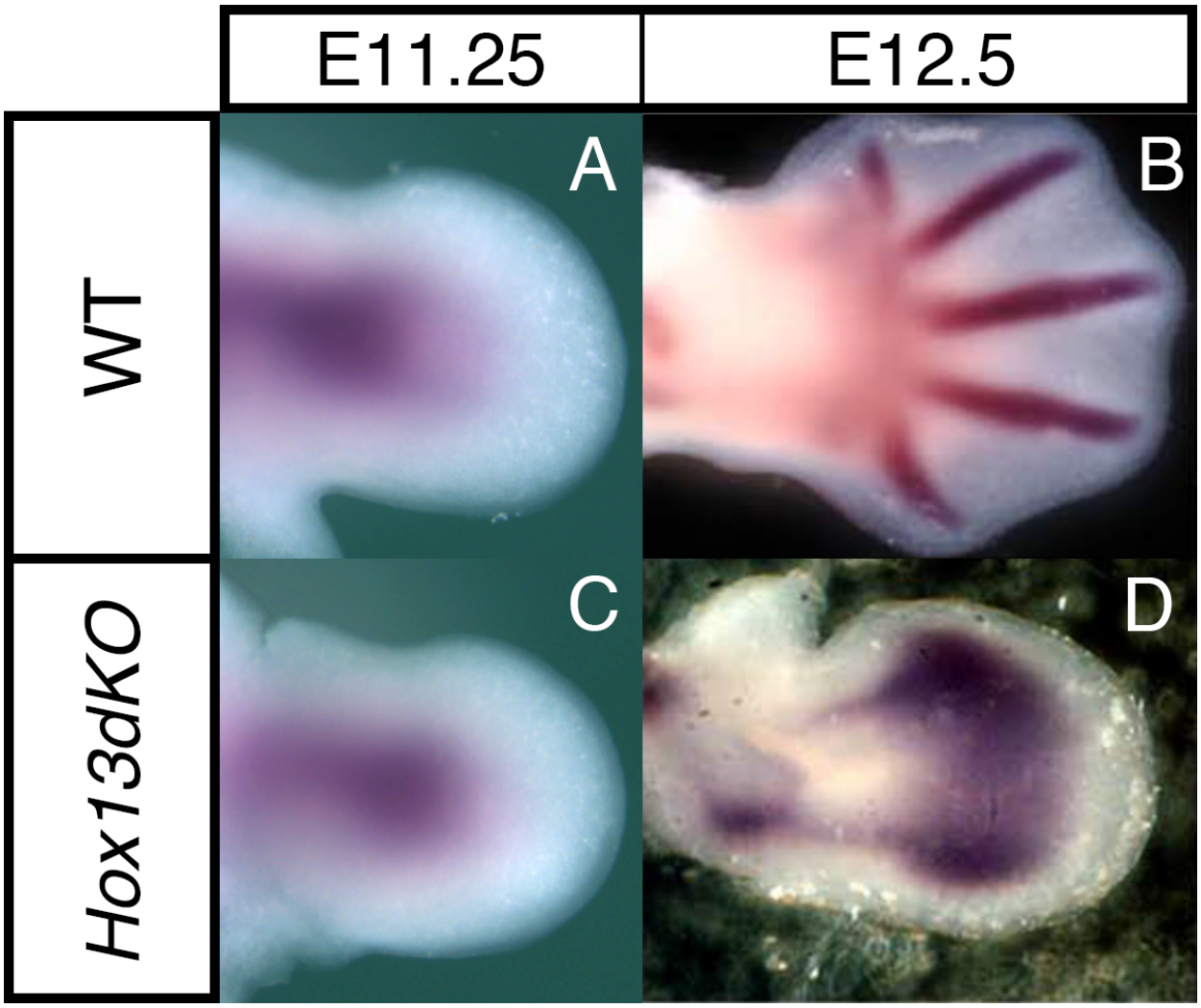

Fig. 12 Cartilage patterning and development are affected in the *Hox13*dKO autopod. Dorsal view of (A) *Col2a1* expression in wild-type and (C) *Hox13*dKO forelimb at E11.25-11.5. Dorsal view of (B) *Col2a1* expression in wild-type and (D) *Hox13*dKO forelimb at E12.5. At E11.25, the *Col2a1* expression pattern and shape of the limb bud is indistinguishable between the wild-type and *Hox13*dKO animals. At E12.5, a single flat cartilaginous condensation without digital structure was observed in the *Hox13*dKO autopod.

RNA from the autopod of wild-type and *Hox13*dKO embryos was isolated and quantified the transcript levels by Genechip (Table 3a, b). To minimize overrepresentation of the genes related to cartilage differentiation caused by loss of the *Hox13* function (Fig. 12) and to concentrate early responding genes to the loss of *Hox13* function, tissue from E11.25 embryos where only the carpal/tarsal anlage had developed in the autopodal region was isolated. In addition, to avoid the effect of stylopod and zeugopod gene expression on changes in their expression in the *Hox13*dKO autopod, the distal autopodal tissue that roughly corresponded to the *Hoxd13* expressing region was isolated.

Of the 781 genes showing upregulation in the E11.25 mutant autopod, 102 genes were included among the CHBRLNr genes (Table 2 and Fig. 13A). Interestingly, genes categorized under “transcription regulation” were enriched in this cluster (P=1.16E-19, 41/102, Table 3c and Fig. 13B). Among the 805 genes showing downregulation in the *Hox13*dKO autopod, 79 genes overlapped with the CHBRLNr genes (Table 2 and Fig. 13A and C). Interestingly, three genes belong to both classes due to their alternate exon usage. Following these analyses, any CHBRLNr genes showing alteration in the *Hox13*dKO were

referred to as direct *Hox* target genes. It is curious that many of the genes exhibiting expression changes in the mutant autopod were not included the CHBRLNr genes. Given that a number of transcription factor-coding genes are HOX13 target, the genes not included in CHBRLNr gene group are likely to be the downstream of *Hox* target transcription factors.

Figure 13

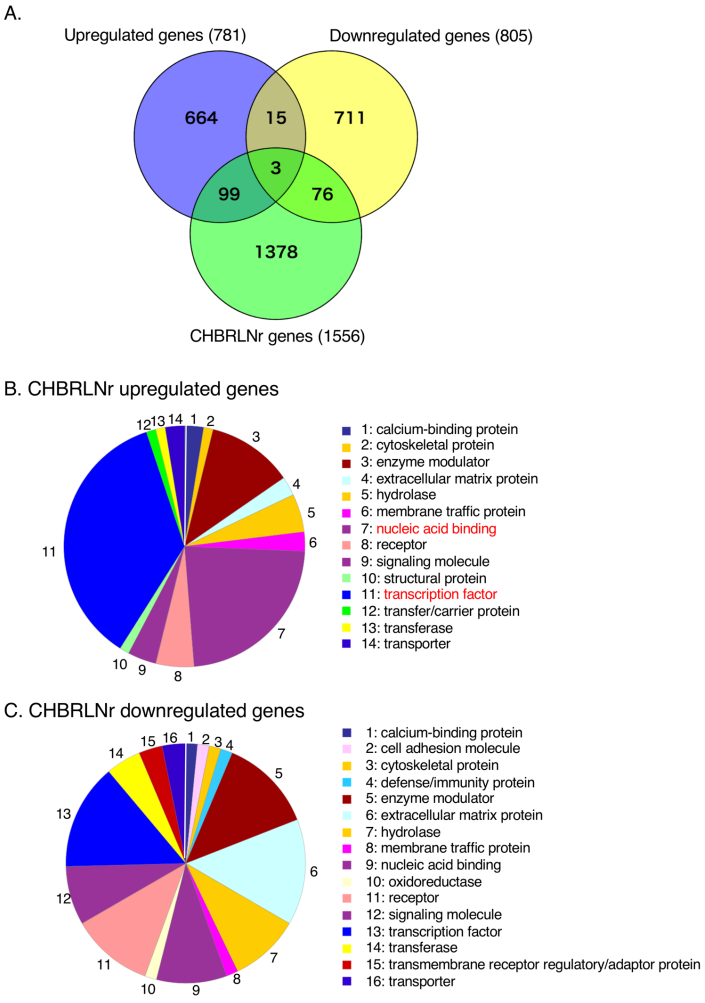

Fig. 13 Profiles of CHBRLNr genes whose expression is altered in *Hox13*dKO autopods. (A) Venn diagram showing the number of CHBRLNr genes exhibiting upregulated or downregulated in the *Hox13*dKO autopods. 18 genes are classified as “Upregulated genes” and “Downregulated genes”. Of these genes, multiple transcripts are generated from single genes due to differences in exon usage. Loss of *Hox13* activity differentially affects the usage of specific exon(s). (B) and (C) show a graphical chart of the functional classification of proteins encoded by CHBRLNr genes that exhibited up- or down-regulation in the *Hox13*dKO autopod, respectively. Red letters in (B) indicate proteins classified under “transcriptional regulation”.

Changes in the spatial expression pattern of HOX11/13 target genes in the *Hox11-13* mutant limb bud

Next, the changes in the spatial expression pattern of HOX11/13 target genes in loss-of-function *Hox13* mutant limb buds was analyzed. In *Hox13*dKO embryos, the cartilage pattern in the limb at E11.25 showed no obvious changes; however, at E12.5 the interdigital region was missing and a single flat cartilage was present instead of the five metacarpi and phalanges (Fig. 12) indicating disorganized patterning of the autopodal cartilage. As representative genes exhibiting altered expression in the *Hox13*dKO limb, *Bmp2*, *Sulf1* and *Stmn2* were chosen as the downregulated genes, and *Aff3*, *Shox2* and *Tshz2* as upregulated genes in the *Hox13*dKO limb. These genes are also common targets of HOXA11, HOXA13, SHOX2, PBX and PITX1 in the limb bud.

Bmp2 was expressed in the mesenchyme of the distal autopod in the wild-type limb and while the expression was not altered in the $Hoxa13^{+/-}$ and $Hoxa13^{-/-}$ limb, it was reduced in the $HoxD^{del(11-13)/del(11-13)}$ and undetectable in the *Hox13*dKO limb bud (Fig. 14A, B and Fig. 15A). *Stmn2* was expressed in the mesenchyme of the anterior autopod

of E11.5 wild-type and *Hoxa13*$^{+/-}$ forelimb buds. The intensity of the autopodal expression signal was not affected in the *Hoxa13*$^{-/-}$, although it was expanded posteriorly in the *HoxD*$^{del(11\text{-}13)/del(11\text{-}13)}$ limb bud. In the *Hox13*dKO limb bud, *Stmn2* expression was undetectable in the autopod (Fig. 14C, D and Fig. 15B).

Sulf1 was expressed in the autopodal mesenchyme of E11.5 wild-type and *Hoxa13*$^{+/-}$ forelimbs. The intensity and area of autopodal expression was decreased in both *Hoxa13*$^{-/-}$ and *HoxD*$^{del(11\text{-}13)/del(11\text{-}13)}$ limbs. The expression signal was further reduced or undetectable in the *Hox13*dKO autopod (Fig. 14E, F and Fig. 15C). *Sulf1* showed dynamic change in the AER expression (Lewandowski et al. 2015) and this expression was affected indirectly by *Hox11-13* mutation (Fig. 14E, F and Fig. 15C, see detail in Fig.15 legend).

Aff3, encoding an AF/FMR2 family transcription factor, was expressed in the E11.5 wild-type zeugopod but not in the autopod. In the E11.5 *Hoxa13*$^{-/-}$ limb, *Aff3* expression was expanded into the autopod and *Aff3* expression was detected in the entire autopodal region of the *Hox13*dKO limb (Fig. 15D, see detail in Fig.15 legend).

Shox2 was expressed in the E11.5 wild-type zeugopod but undetectable in the autopod, and the expression was not affected in E11.5 *HoxD*$^{del(11\text{-}13)/del(11\text{-}13)}$ and *Hoxa13*$^{-/-}$ mice (Fig. 15E). In contrast, in the E11.5 *Hox13*dKO mice, *Shox2* expression was expanded into the posterior autopodal region (Fig. 14G, H, arrowhead).

Tshz2 is expressed in the E11.5 zeugopodal mesenchyme but not in the autopod (Caubit et al. 2000). Ectopic *Tshz2* expression was detected in the distal and posterior periphery of the E11.5 *Hox13*dKO autopod (Fig. 14I, J, arrow). However, this aberrant expression pattern was not observed in *Hoxa13*$^{-/-}$ or *HoxD*$^{del(11\text{-}13)/del(11\text{-}13)}$ mice (Fig. 15F). Thus, genes that exhibited altered expression levels in the *Hox13*dKO autopod in Genechip analysis actually showed unique changes in the spatial expression pattern in the *Hox13*dKO limb bud.

The expression of the *Hox13* target transcription factors, *Aff3*, *Bnc2*, *Nfib* and *Runx1t1* whose expression was increased in the *Hox13*dKO autopod was further analyzed. Of these, *Aff3*, *Bnc2* and *Runx1t1* are common target genes of HOXA11, HOXA13, SHOX2, PBX and PITX1 whereas *Nfib* is a common target gene of HOXA11, HOXA13 and PITX1

in the limb bud. *Aff3*, *Bnc2*, *Nfib* and *Runx1t1* were expressed in the zeugopodal mesenchyme and cartilage but not in the autopod at E11.5 (Fig. 16B, G, L, Q). Expression of these genes was then also detected in the autopodal cartilage or perichondrium at E12.5 (Fig. 16D, I, N, S). In the *Hox13*dKO embryos at E11.5, the expression of *Aff3*, *Bnc2*, *Nfib* and *Runx1t1* were clearly expanded into the autopod (Fig. 16C, H, M, R). Thus, representative *Hox* target genes exhibiting increased transcription in the *Hox13*dKO by Genechip were confirmed to be ectopically transcribed in the autopodal mesenchyme in the *Hox13*dKO. The expression of these genes in the zeugopod mesenchyme was already detectable at E10.5 when zeugopodal cartilage formation is just beginning (Fig. 16A, K, P) except *Bnc2*. In contrast, expression of these genes was suspended in the autopod mesenchyme at E11.5. Thus, the relationship between the expression of these genes in the mesenchyme and cartilage is different between the zeugopod and autopod.

Thus, a change in the level of a transcripts of a representative gene in the *Hox13*dKO autopod shown by Genechip analysis was verified by WISH analysis.

Figure 14

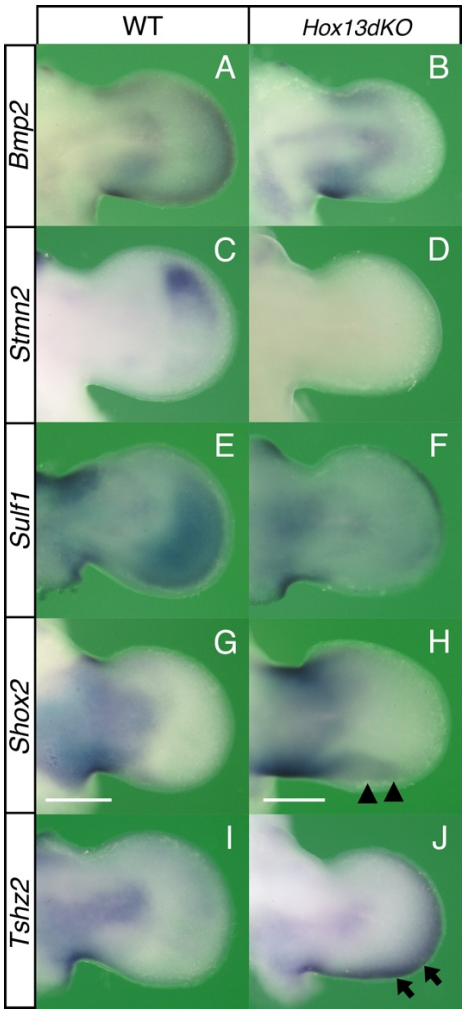

Fig. 14 Altered gene expression patterns in the *Hox13*dKO autopod. Dorsal view of gene expression detected by *in situ* hybridization in E11.25-11.5 (A, C, E, G, I) wild-type and (B, D, F, H, J) *Hox13*dKO forelimb buds. The expression of (A and B) *Bmp2*, (C and D) *Stmn2* and (E and F) *Sulf1* in the autopodal mesenchyme was reduced or undetectable in the *Hox13*dKO embryos. In contrast, (G and H) *Shox2* and (I and J) *Tshz2* showed ectopic expression in the *Hox13*dKO autopod. Since *Hoxa13* KO mice was generated by inserting *Neo* sequence in *Hoxa13* locus, *Neo* expression mimics *Hoxa13* expression. In order to define the autopod as the region expressing *Hoxa13* in the *Hox13*dKO mice, contralateral limb bud of each specimen was hybridized with *Neo* probe (results not shown). Scale bar indicates 500 μm.

Figure 15

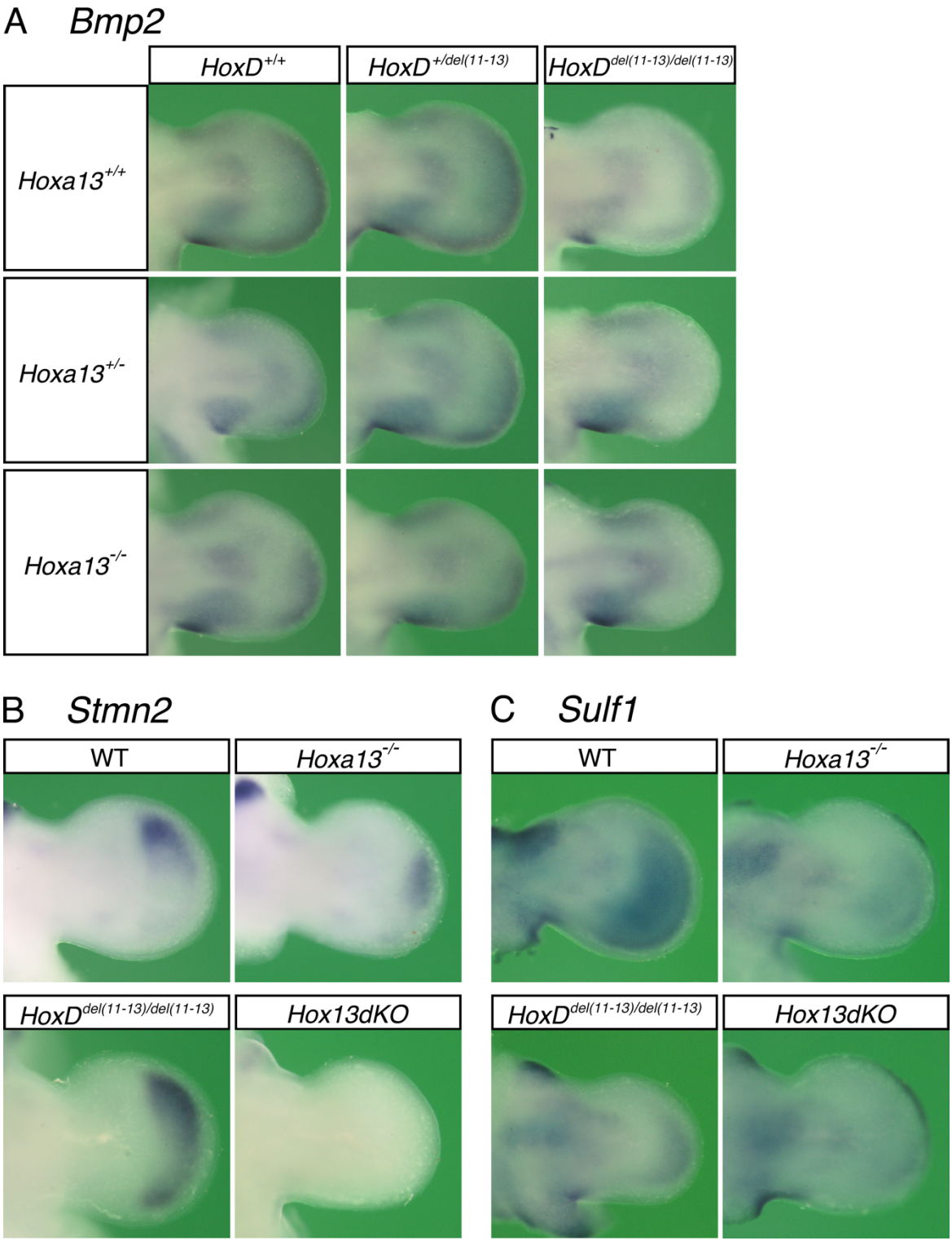
A Bmp2
HoxD+/+
HoxD+/del(11-13)
HoxDdel(11-13)/del(11-13)
Hoxa13+/+
Hoxa13+/-
Hoxa13-/-
B Stmn2
WT
Hoxa13-/-
HoxDdel(11-13)/del(11-13)
Hox13dKO
C Sulf1
WT
Hoxa13-/-
HoxDdel(11-13)/del(11-13)
Hox13dKO

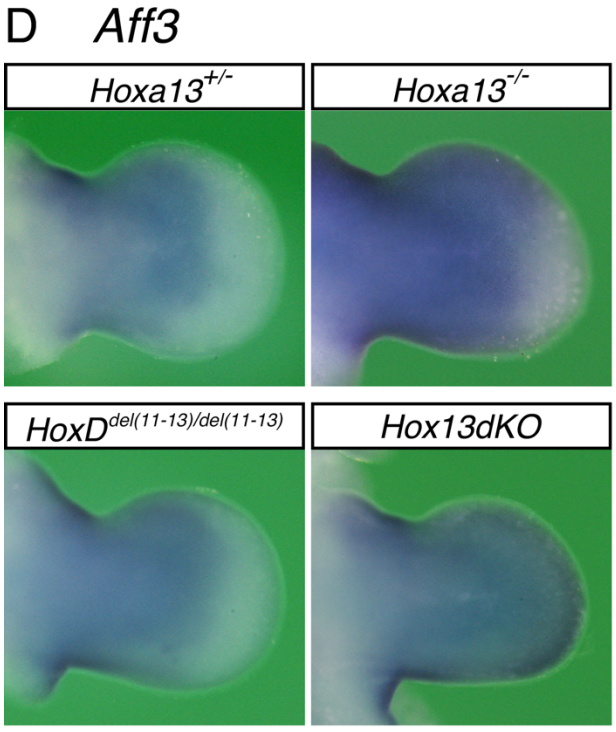
D Aff3
Hoxa13+/-
Hoxa13-/-
HoxDdel(11-13)/del(11-13)
Hox13dKO

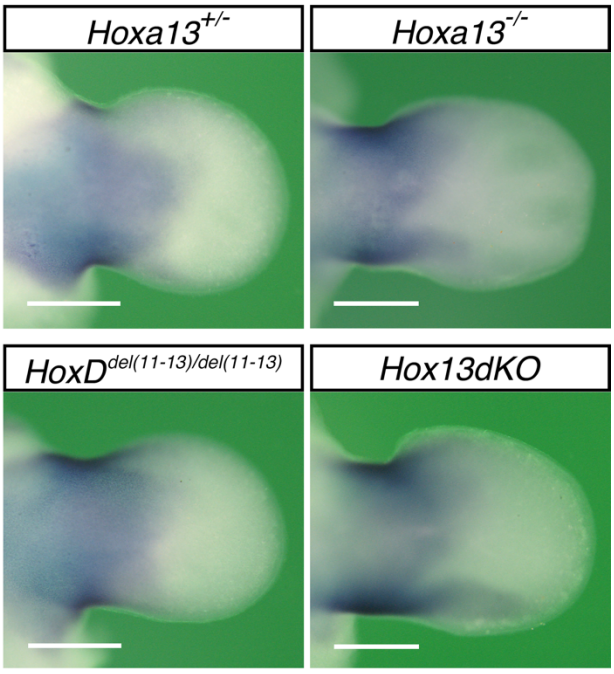
E Shox2
Hoxa13+/-
Hoxa13-/-
HoxDdel(11-13)/del(11-13)
Hox13dKO

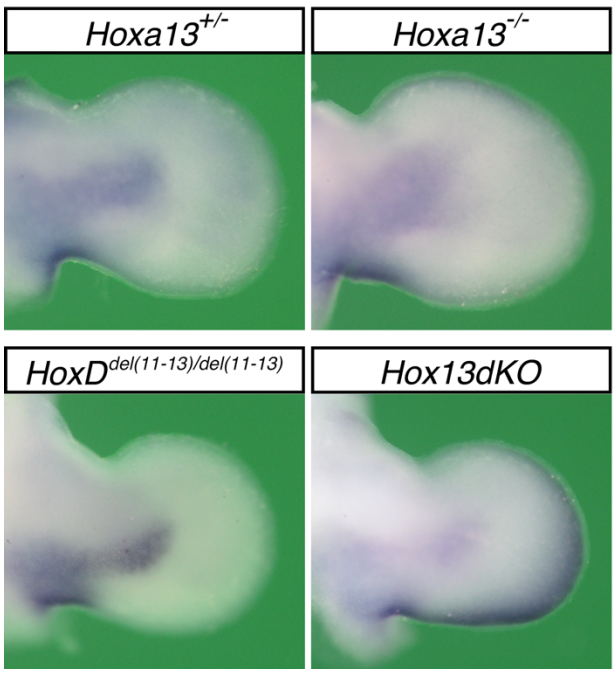
F Tshz2
Hoxa13+/-
Hoxa13-/-
HoxDdel(11-13)/del(11-13)
Hox13dKO

Fig. 15 Variation in HOXA13 regulatory roles in target gene expression. Dorsal view of gene expression in the forelimb bud visualized for (A) *Bmp2*, (B) *Stmn2*, (C) *Sulf1*, (D) *Aff3*, (E) *Shox2* and (F) *Tshz2* around E11.25. Fig. 14 shows the expression in wild-type and *Hox13*dKO embryos. Results for all genotype combinations for *Bmp2* and results from single homozygotes for *Sulf1*, *Stmn2*, *Aff3*, *Tshz2* and *Shox2* are presented. Wild-type and *Hox13*dKO images are the same as presented in Fig.14. (A) *Bmp2* expression in the anterior distal autopod was *Hoxa13* dependent. *Hoxa13* was expressed in this region but *Hoxd11-13* were not expressed indicating that *Bmp2* expression in this region is *Hoxa13* dependent. In contrast, *Bmp-2* expression in the posterior- and central-distal region of the limb bud decreased as *Hox11-13* gene dosage decreased. (B) Intense expression of *Stnm2* was observed in the anterior autopod and weaker expression was detected in the posterior autopod. The intense *Stmn2* expression domain "shifted" to the distal most autopod in the $Hoxa13^{-/-}$ limb. In contrast, the posterior expression was strengthened in the $HoxD^{del(11-13)/del(11-13)}$ limb and undetectable in the *Hox13*dKO limb indicating the presence of a complicated regulatory mechanism possibly involving additional transcription factors downstream of *Hox*. (C) Mesenchymal *Sulf1* expression in the autopod showed *Hox* gene dose dependence. *Sulf1* is also expressed in the AER at E10.5, then the expression gradually decreased from posterior to anterior direction, finally the expression disappears at E11.5 (additional data deposited in Mouse Genome Information (Lewandowski et al. 2015)). In $Hoxa13^{-/-}$ limb bud, this change in the expression is delayed or suppressed in the anterior AER. Interestingly, this change was not observed in $HoxD^{del(11-13)/del(11-13)}$ limb buds and the expression in the *Hox13*dKO limb buds was indistinguishable from that of $Hoxa13^{-/-}$ limb buds. These evidences indicate that the regulation of AER-*Sulf1* expression is specific to *Hoxa13.* (D) The expression of *Aff3* was not altered in the $HoxD^{del(11-13)/del(11-13)}$. In contrast, *Aff3* expression was expanded to the autopodal region in the $Hoxa13^{-/-}$ embryos leaving the distal posterior region without expression. Uniform *Aff3* expression was observed in the autopod of the *Hox13*dKO indicating that HOXA13 represses *Aff3* expression in the anterior autopod and HOXA13 and HOXD11-13 repress *Aff3* expression in a dose-dependent manner in the posterior autopod. (E) *Shox2* expression was not altered in either $Hoxa13^{-/-}$ or $HoxD^{del(11-13)/del(11-13)}$ whereas ectopic autopodal expression at the posterior margin was observed in the

*Hox13*dKO indicating that *Hoxa13* and *Hoxd11-13* redundantly repress the *Shox2* expression. (F) *Tshz2* expression was not altered in either the *Hoxa13*$^{-/-}$ or *HoxD*$^{del(11-13)/del(11-13)}$, whereas ectopic expression in the autopodal distal margin was observed in the *Hox13*dKO, indicating that *Hoxa13* and *Hoxd11-13* redundantly repress *Tshz2* expression in the E11.5 autopod. Scale bar indicates 500 μm.

Figure 16

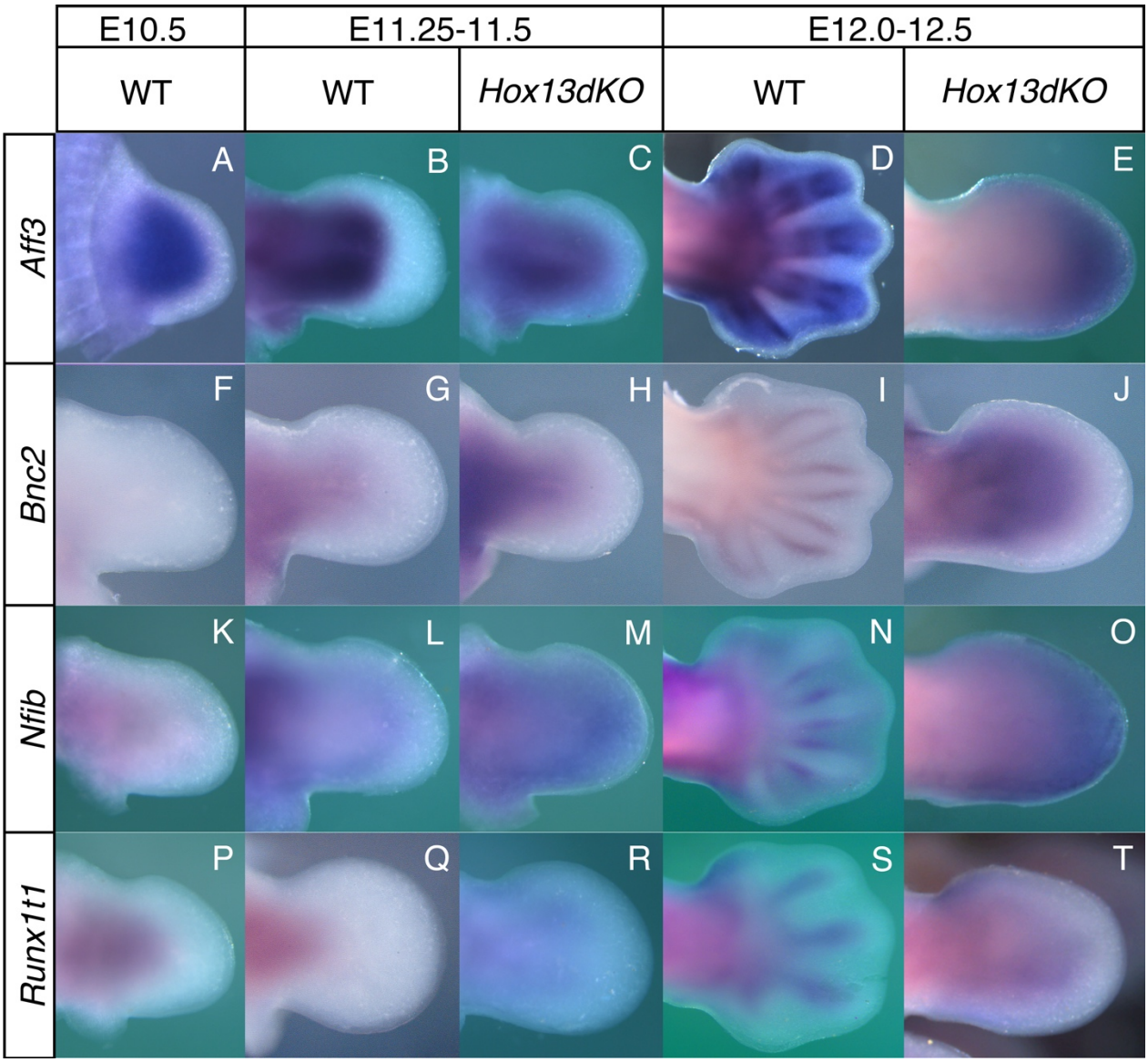

Fig. 16 Transition in the spatial expression pattern of the genes encoding *Hox* target transcription factors associated with cartilage differentiation and changes in the *Hox13*dKO autopod. Dorsal view of gene expression detected by *in situ* hybridization in the forelimb bud at (A, F, K, P) approximately E10.5, (B, C, G, H, L, M, Q, R) E11.5 and (D, E, I, J, N, O, S, T) E12.5. (A) In wild-type embryos, *Aff3* was expressed throughout the entire limb bud mesenchyme excluding the narrow distal most region at E10.5. *Aff3* expression was not found in the autopod at (B) E11.5; however, at (D) E12.5 expression was detected in the cells in/around the perichondrium of the autopod but not in the

interdigital mesenchyme. In *Hox13*dKO embryos, *Aff3* expression expanded to the proximal autopodal region (C) at E11.5 then the expression was observed throughout the entire autopodal mesenchyme (E) at E12.5. *Bnc2* expression was not detected in the (F) E10.5 mesenchyme but was detected in the center of the stylopod and zeugopod (G) at E11.5. (I) *Bnc2* expression was later found in the perichondrium of the limb cartilage including the autopod at E12.5. *Bnc2* expression was expanded to the proximal *Hox13*dKO autopod (H) at E11.5 and throughout the entire mesenchyme (J) at E12.5. *Nfib* expression was found in the proximal region of the (K) E10.5 limb bud then in the zeugopod/autopod boundary region at (L) E11.5. (N) *Nfib* expression was detected in the perichondrium of the autopodal cartilage at E12.5. In the *Hox13*dKO limb bud, expression was detected throughout the entire autopodal mesenchyme both (M) at E11.5 and (O) E12.5. *Runx1t1* expression was detected in the proximal center of the (P) E10.5 and (Q) E11.5 limb but excluded from the autopodal region. (S) In the E12.5 autopod, *Runx1t1* expression was detected in the cartilaginous condensation. In *Hox13*dKO embryos, *Runx1t1* expression was expanded to the proximal autopod at (R) E11.5 and the central region of the autopod showed expression at (T) E12.5.

Changes in the *Hox11/13* target gene expression patterns in the *Ulnaless* limb bud

As shown, autopodal expression of a group of the *Hox11/13* target genes such as *Aff3*, *Shox2* and *Tshz2* at E11.5 are probably transiently repressed by *Hox13*. To verify this possibility, the effect of *Hoxd13* mis-expression was analyzed. For this purpose, *Ulnaless* (*Ul*), which is a dominant mutation of the *HoxD* locus caused by a chromosomal inversion which results in the truncation of both the ulna and fibula due to mis-expression of *Hoxd13* in the posterior zeugopod (Peichel et al. 1997) was adopted.

In the E11.5 *Ul*/+ mice, *Tshz2* expression in the distal zeugopod was reduced and the expression domain was narrowed at the dorsal zeugopodal region and reduced in the ventral zeugopod (Fig. 17A), and *Shox2* expression was weakened at the dorsal posterior and ventral region of the zeugopod (Fig. 17B). In the E12.5 *Ul*/+ mice, the *Aff3* signal was undetectable specifically in the ventral zeugopodal region (Fig. 17C, arrow). Thus, the expression of these genes in the zeugopod was downregulated in the ectopic *Hoxd13* domain confirming that *Hoxd13* is repressive against the expression of these genes.

Figure 17

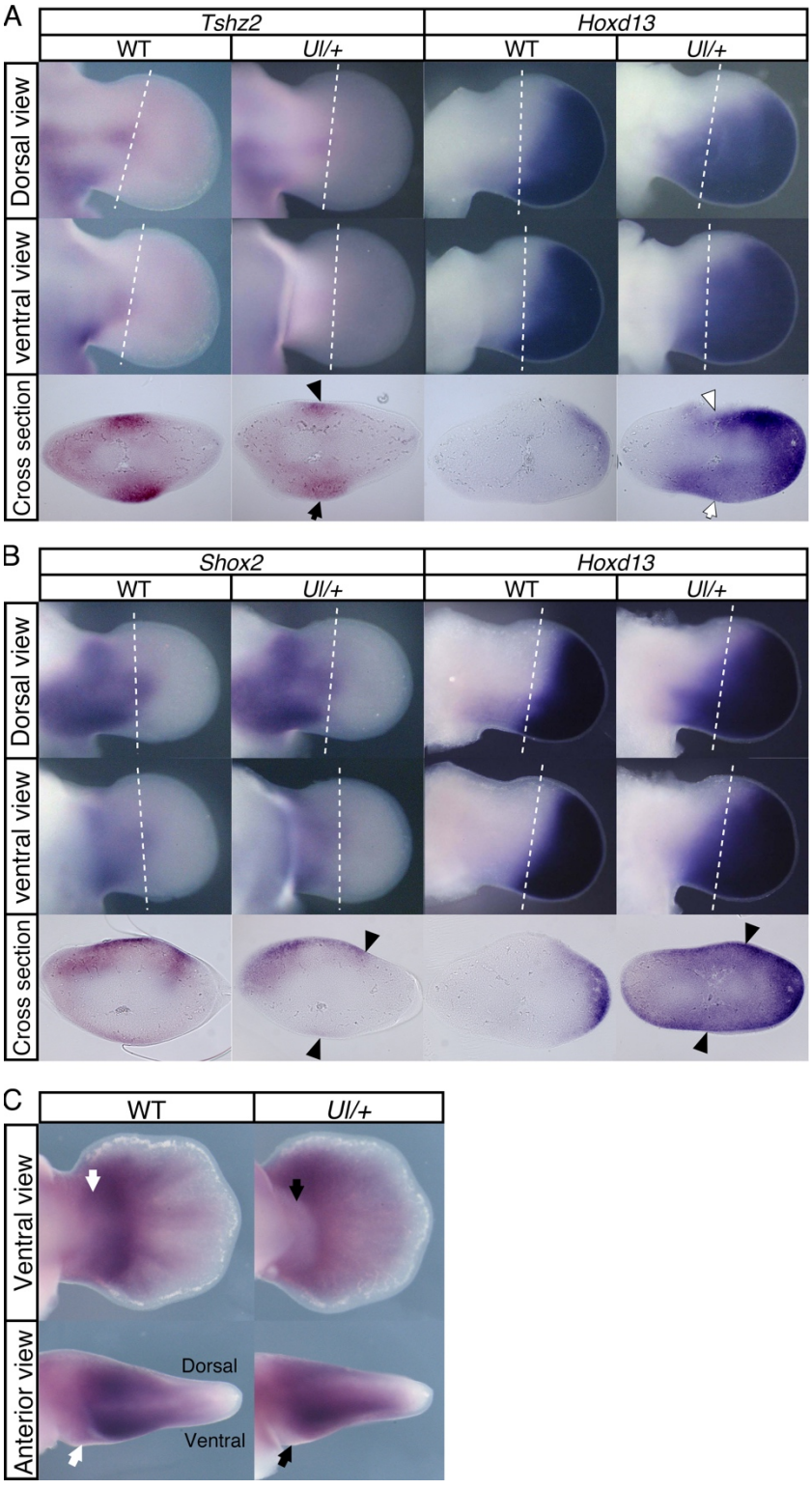
A
Tshz2
Hoxd13
WT
Ul/+
WT
Ul/+
Dorsal view
ventral view
Cross section
B
Shox2
Hoxd13
WT
Ul/+
WT
Ul/+
Dorsal view
ventral view
Cross section
C
WT
Ul/+
Ventral view
Anterior view
Dorsal
Ventral

Fig. 17 In the *Ulnaless* limb, ectopic *Hoxd13* expression represses target gene expression. Expansion of the *Hoxd13* expression domain to more a proximal area overlapping with the zeugopodal region occurred in the *Ul/+* mutant limb. Reduction of (A) *Tshz2*, (B) *Shox2* and (C) *Aff3* expression in the zeugopod region overlapping the ectopic *Hoxd13* expression domain indicates that *Hoxd13* as well as *Hoxa13* represses the expression of these genes. (A) The black arrow and arrowhead indicate the reduced *Tshz2* expression and the white arrow and arrowhead indicate ectopic *Hoxd13* expression. (B) Black arrowheads indicate the tissues with reduced expression of *Shox2* and augmented *Hoxd13* expression. (C) Black arrows indicate the reduction in *Aff3* expression in the *Ul/+* limb and the white arrows indicate the corresponding region in the wild-type limb. Dotted lines in A and B indicate the position of cross sections. Ventral views were digitally inverted (left-right). In the panel A and B, the left and right limb buds were isolated from a single embryo at E11.5 and were hybridized with *Tshz2* or *Shox2* probe and *Hoxd13* probe, respectively.

HOXA13 represses cartilage differentiation of limb mesenchymal cells through BCL11a

Bcl11a encodes a zinc finger-type transcriptional repressor (Liu et al. 2003) whose expression was decreased in the *Hox13*dKO autopod. BCL11a represses blood cell differentiation (Liu et al. 2003), however its function in cartilage differentiation remains elusive.

Bcl11a was expressed throughout the entire limb mesenchyme at E10.5 (Fig. 18A), then at E11.5 the expression was detected in the autopodal mesenchyme and the posterior zeugopodal mesenchyme (Fig. 18B). At E12.0 the expression was found in the perichondrium of the autopodal cartilage (Fig. 18D) where *Hoxa13* was also expressed. As expected from Genechip analysis, expression was severely decreased in the E11.5 autopodal mesenchyme of the *Hox13*dKO (Fig. 18C). Interestingly, *Bcl11a* expression reappeared in the *Hox13*dKO autopod at E12.0 where the single flat cartilage was forming instead of the five metacarpi and phalanges (Fig. 18E).

Then the effect of *Bcl11a* overexpression on the differentiation of the limb

mesenchymal cells into cartilage was analyzed using a micromass culture system and monitoring Col II expression as a marker of differentiation (Fig. 18F-H). The effect of another family gene, *Bcl11b,* that is expressed in the limb mesenchyme (result not shown) and has both HOXA11 and HOXA13 binding sites (Table 2) was also analyzed. As shown in Fig. 9I and J, the expression level of Col II was reduced to 53% and 49% in the *Bcl11a* and *Bcl11b* transfected cells, respectively, compared to non-transfected cells at day 1. At day 2, the expression of Col II in *Bcl11a* and *Bcl11b* transfected cells was also reduced to 63% and 48%, respectively (Fig. 18K, L). Thus, similar to blood cell differentiation, both BCL11a and BCL11b have repressive activity on the cartilage differentiation of mesenchymal cells of the limb bud. Taken together, HOXA13 represses limb cartilage differentiation at E11.5.

Figure 18

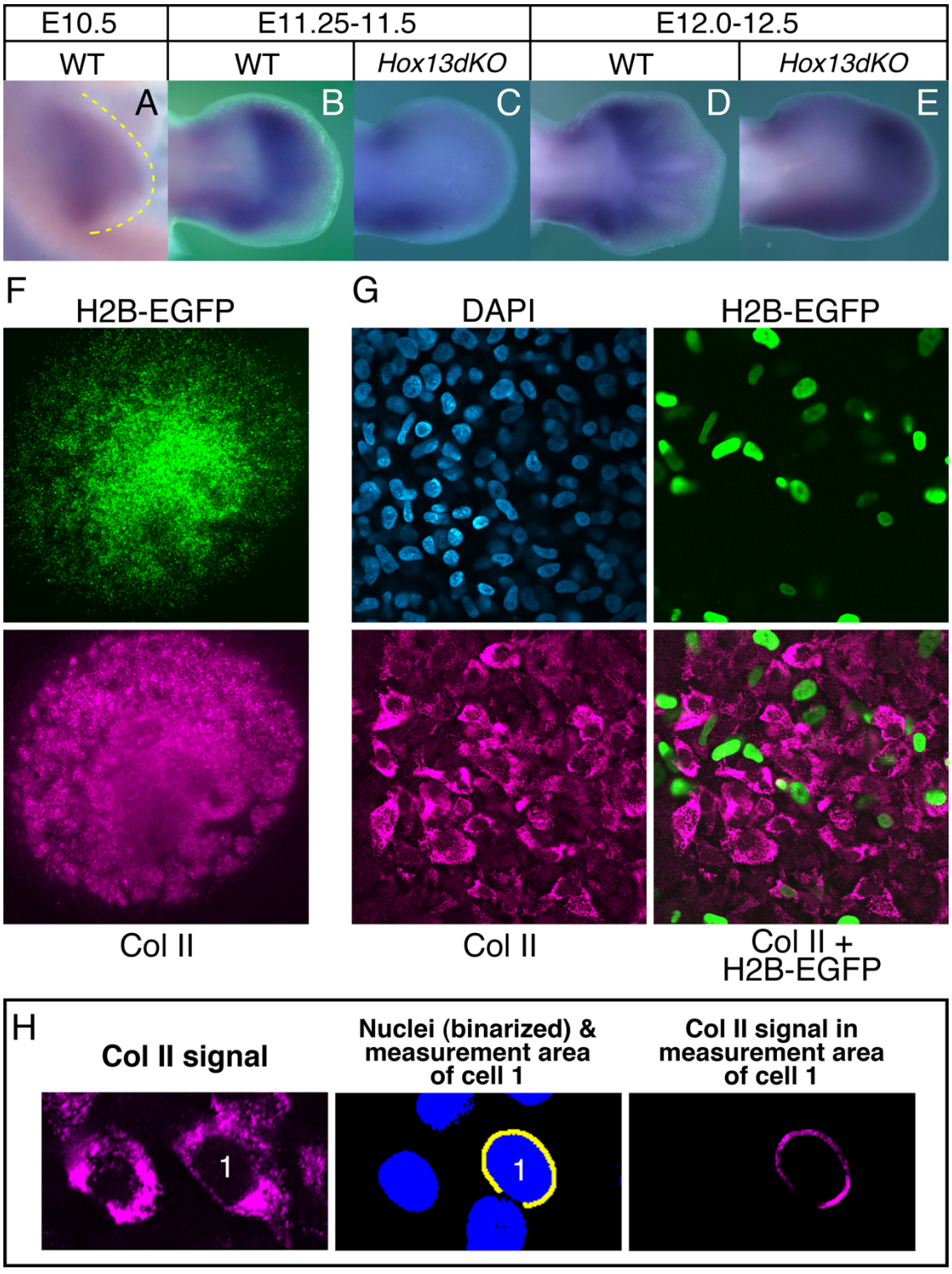
E10.5
E11.25-11.5
E12.0-12.5
WT
WT
Hox13dKO
WT
Hox13dKO
A
B
C
D
E
F
H2B-EGFP
G
DAPI
H2B-EGFP
Col II
Col II
Col II +
H2B-EGFP
H
Col II signal
Nuclei (binarized) &
measurement area
of cell 1
Col II signal in
measurement area
of cell 1
1
1

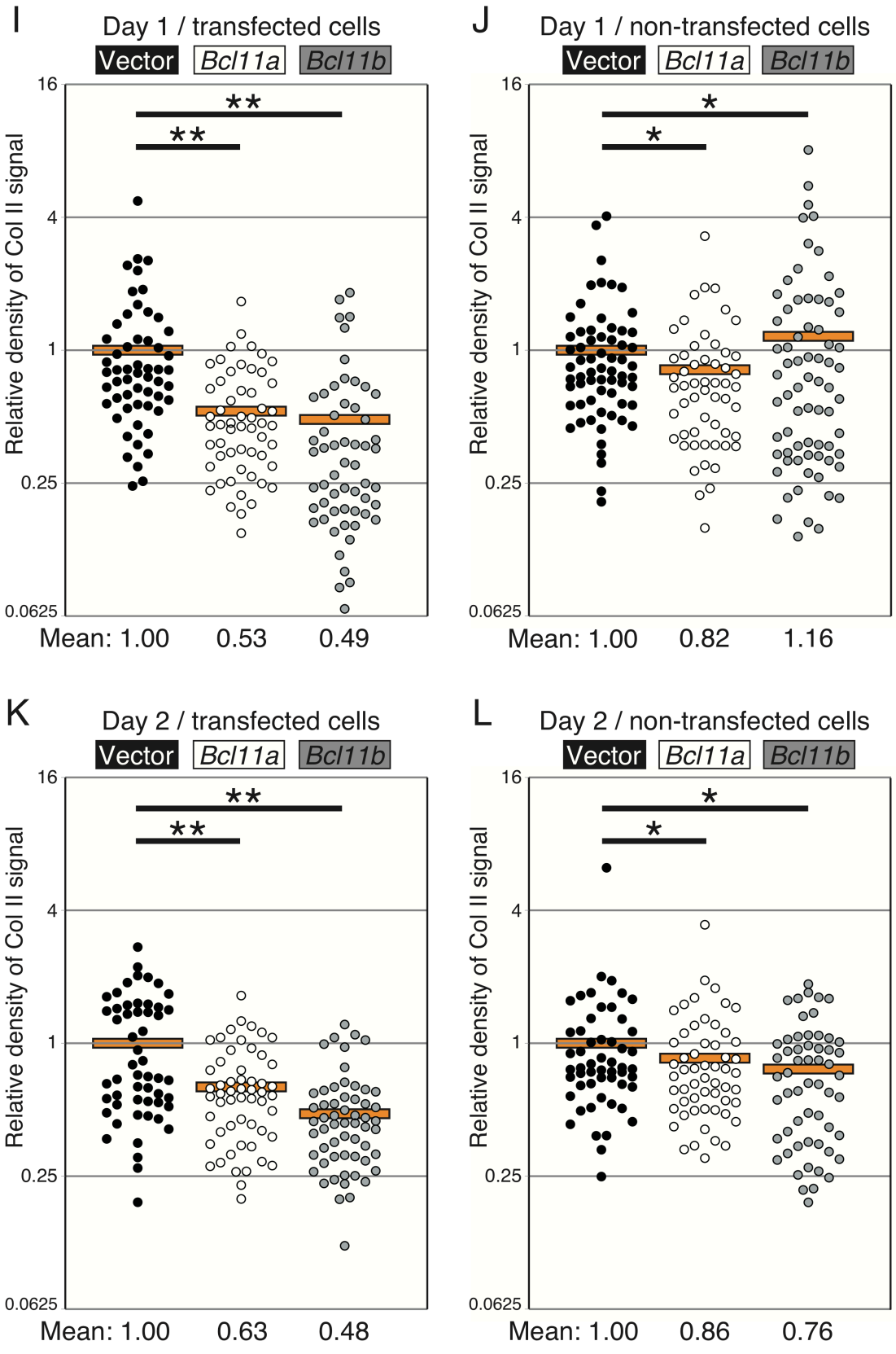
I
Day 1 / transfected cells
Vector
Bcl11a
Bcl11b
Relative density of Col II signal
16
4
1
0.25
0.0625
**
**
Mean: 1.00
0.53
0.49
J
Day 1 / non-transfected cells
Vector
Bcl11a
Bcl11b
Relative density of Col II signal
16
4
1
0.25
0.0625
*
*
Mean: 1.00
0.82
1.16
K
Day 2 / transfected cells
Vector
Bcl11a
Bcl11b
Relative density of Col II signal
16
4
1
0.25
0.0625
**
**
Mean: 1.00
0.63
0.48
L
Day 2 / non-transfected cells
Vector
Bcl11a
Bcl11b
Relative density of Col II signal
16
4
1
0.25
0.0625
*
*
Mean: 1.00
0.86
0.76

Fig. 18 BCL11a and BCL11b repress cartilage differentiation in micromass culture (MMC).

(A) *Bcl11a* was expressed throughout the entire mesenchyme of the limb bud at E10.5 then became restricted to the autopod and anterior and posterior margin of the more proximal part of the limb (B) at E11.5. *Bcl11a* expression was detected in the interdigital region (D) at E12.0. In the *Hox13*dKO limb (C) at E11.5, autopodal expression was severely reduced but (E) at E12.5 uniform expression was detected throughout the autopod. (F) Histone H2B-EGFP (H2B-EGFP) fluorescence and Col II immunofluorescence signals in MMCs incubated for 2 days after transfection with the pCAGGS-*H2B-EGFP* and pCAGGS vector. (G) High magnification confocal images of the MMC in panel F. Nuclei of the transfected cells were marked with H2B-EGFP. (H) For quantitative analyses of Col II expression in each cell, the intensity of the Col II immunofluorescence signal in the ring-shaped area (yellow; width: 0.58 μm) around each nucleus (green) was calculated using ImageJ. Neighboring nuclear areas were excluded from the measurement area. (I-L) Ratios of Col II immunofluorescence signal intensity in each cell relative to the mean of the vector transfection control. I, J: 1-day incubation; K, L: 2-day incubation. I, K: transfected cells (H2B-EGFP-positive); J, L: non-transfected cells (H2B-EGFP-negative). In the graphs, a circle represents one cell, and n $\approx$ 60 for each transfection. **: $p < 0.002$; *: $p > 0.01$ (Mann-Whitney U test). Orange bars indicate the mean of the values.

Discussion

To elucidate the mechanism controlling region-specific morphogenesis of the zeugopod and autopod, direct target genes of HOXA11 and HOXA13 in the limb bud were identified. It was found that HOXA11and HOXA13 regulate their common target genes involved in cartilage differentiation in distinct way, where HOXA13-dependent regulation appears to be central to generating pentadactylous (five digits) autopod.

ChIP-Seq analysis is a technique for identification of *Hox* target genes. Using the same HOXA13 antibody as in this study, it has been shown that HOXA13 regulates autopod-specific expression of *Hoxd13* through direct binding to the digit-specific enhancer (Beccari et al. 2016). Sheth et al. (Sheth et al. 2016) identified the limb target genes of HOXA13 and HOXD13, whose function is redundant in the autopodal development. They reported most of the target genes are common to both HOXA13 and HOXD13 and many of them are related to cartilage differentiation. Further extraction and elucidation of the crucial genes from these many candidate genes are current subjects. Jerkovic et al. (Jerkovic et al. 2017) attempted to identify the *Hox* target genes by ChIP-

Seq analysis after forced expression of paralogous *Hox* genes in cultured chicken limb bud mesenchymal cells. They found that common HOX binding site and a group of HOX proteins interact with CTCF. Since this analysis was performed using cultured cells and overexpression of tagged HOX protein, the results need to be verified by using a more native system. A loss-of-function phenotype for *Hox11* was observed in the zeugopod and proximal autopod, and for *Hox13* in the autopod. In both cases, hypomorphic cartilage development was observed indicating the presence of common target genes responsible for chondrogenic differentiation from limb bud mesenchymal cells. In this study, mesenchymal cells from mouse limb bud and antibodies against HOXA11 or HOXA13 were used for this ChIP-Seq analysis to narrow down the common *Hox* target genes that are critical for chondrogenic differentiation. Based on the analysis of these target genes, the unique role of *Hox13* in the autopod-specific gene regulation network was revealed.

HOX11/13, SHOX2 and PITX1 share common targets

It was shown that most of the HOXA11 ChIP-Seq peaks overlapped with the

HOXA13 peaks (Fig. 3-5) and many of the genes neighboring the common peak are involved in cartilage differentiation (Fig. 11A). Since *Hoxa11* and *Hoxa13* are expressed in the zeugopod and autopod, respectively, except carpal/tarsal region (Fig. 1 and 2), each HOX11/13 binds to a common sequence in their unique expression domain and are expected to control the target gene expression in an expression domain-specific manner. In addition, non-HOX homeodomain transcription factors are shown to bind to the same region in the common HOX11/13 binding domain of the limb bud.

There are accumulating evidences that Hox and non-Hox homeodomain transcription factors coordinate during limb cartilage development. *Pitx1* encodes a paired-like homeodomain transcription factor whose expression in the limb bud is restricted to the hindlimb and functions to transform forelimb type morphogenesis to hindlimb type morphogenesis (Lanctot et al. 1999). Both the fore- and hindlimbs have basically the same topological architecture of the bone and differences in their morphology are thought to be based on quantitative rather than qualitative variation in gene expression or temporal differences in expression of common genes functioning in the limb cartilage

development. The expression of *Hox* and *Pitx1* in the mesenchyme of the hindlimb bud is largely overlapping (Shang et al. 1997). In the present study, it was found that many ChIP-Seq proximal genes are shared by HOX11/13 and PITX1 (Fig. 3 and 4) and that many of these genes are involved in cartilage differentiation (Fig. 11D), These indicate that PITX1 also participates in directly regulating cartilage differentiation in collaboration with HOX11/13. Since the *Hox* expression pattern in the fore- and hindlimb bud is very similar, binding of PITX1 to the HOX11/13 common binding region (CHBRLs) could modulate HOX function. One plausible molecular mechanism for the interplay between PITX1 function and HOX11/13 is that binding of PITX1 to some HBSs of multiple HBSs in the enhancer results in fine tuning of the transcriptional frequency or timing in a program characteristic to that of the hindlimb bud. Given that CHBRLs potentially include multiple HBSs (Fig. 7 and 9I-L), analysis of interaction of multiple transcription factors in combination with CHBRL sequences will provide new insights into the complex regulatory processes centered by HOX13.

Another interesting example on functional coordination with *Hox* is *Shox2* that encodes a

paired-like homeodomain transcription factor. Mice with a loss of *Shox2* function exhibited severe truncation of the stylopod bone of fore- and hindlimbs in addition to hypoplasia of the hindlimb zeugopodal bone (Cobb et al. 2006;Bobick and Cobb 2012). *Shox2* showed overlapping expression with *Hoxa9-11* in the mesenchyme of the stylopod and zeugopod then in the outer layer of the perichondrium and proliferating chondrocytes but not in the autopod (Swinehart et al. 2013;Neufeld et al. 2014). Genetic analysis revealed that *Shox2* is a downstream gene of *Hox11* (Gross et al. 2012). It was found that HOXA11 binds to one of the *Shox2* limb-specific enhancers (Fig. 4C and Fig. 7) indicating the possibility that HOXA11 directly control region-specific expression of *Shox2* in the limb buds through binding to this enhancer/CHBRL. HOXA13 also binds this CHBRL (Fig. 4C and Fig. 7) and *Shox2* is mis-expressed in the *Hox13*dKO (Fig. 11G, H) suggesting that binding of HOXA13 to this enhancer is involved in repressing *Shox2* expression in the autopod. SHOX2 also bind to this CHBRL (Fig. 4C) indicating that SHOX2 participate self-regulation in coordination with HOX11. Interestingly, genetic analysis also suggested that *Hox* and *Shox2* coordinate during development of the stylopodal and zeugopodal cartilage

(Neufeld et al. 2014). Supporting this observation, it was shown that SHOX2 also shares common binding regions of some *Hox* target genes with HOXA11 and HOXA13 (Fig. 3-5, and Table 2). Genes involved in the skeletal development, such as *Aff3*, *Bmp2*, *Bnc2* and *Runx1t1* were concentrated in these common genes (Fig. 11B). These indicate the possibility that SHOX2 and HOXA11coordinately regulate these gene expression through the CHBRLs in the zeugopod by the similar mechanism as the PITX1 and HOXA11. Thus, HOXs regulate multiple steps in the SHOX2 functional cascade during cartilage development along the proximodistal axis of the limb.

On the HOX binding to the *Hoxa11* intron

The binding profiles of HOXA11, HOXA13 and other homeodomain transcription factors to the HoxA cluster are different (Fig. 3A). Both HOXA11 and HOXA13 bind to the 5' untranslated region (5'-UTR) of the *Hoxa9* and *Hoxa7* intron. However, while HOXA13 binds to the *Hoxa11* intronic region, the binding of HOXA11 to the *Hoxa11* intron is minimal or negligible (Fig. 3A). This indicates that in the autopod, HOXA13 binds to the

Hoxa11 intron but HOXA11 shows little or no binding to the *Hoxa11* intron in the zeugopodal anlage. *Hoxc10* is expressed in the mesenchyme of the stylopodal and zeugopodal anlagen of the hindlimb bud. Using deposited ChIP-Seq data (Jain et al. 2018), it was found that HOXC10 also binds to the *Hoxa7* intron and *Hoxa9* 5'-UTR but binding to the *Hoxa11* intron was significantly lower or indistinguishable from background (Fig. 19). Interestingly, non-HOX homeodomain transcription factors SHOX2 and PBX also exhibited similar binding profiles to the *Hoxa11* intron (Fig. 3A). HOXA13 and HOXD13 bind to the "digit enhancer" in the *Hoxa11* intron and activate transcription from the promoter in the first exon of *Hoxa11* in the opposite direction as *Hoxa11* transcription. This counter directional transcription itself is important to inactivate *Hoxa11* transcription in the autopod (Kherdjemil et al. 2016). Based on the observation that *Hoxa11* and *Hoxa13* are co-expressed in the distal fin bud of fish and that forced mis-expression of *Hoxa11* in the autopodal anlage in the mouse causes polydactyly, the system that represses *Hoxa11* expression in the autopod of tetrapods is expected to have been acquired during the evolutionary transition from polydactyly to pentadactyly (Kherdjemil et

al. 2016). Like most of the CHBRL, multiple and evolutionarily conserved HBSs are present in the *Hoxa11* intronic “digital enhancer” (Fig. 20). As described, compared to other common HOX11/13 binding regions, the binding to the *Hoxa11* intron is very specific to HOXA13. It is possible that novel transcriptional co-factor(s) specifically interacts with HOXA13 to stabilize HOXA13 binding to the HBS(s) in the *Hoxa11* intronic “digital enhancer”. These suggest that in addition to the recruitment of the HOX binding sequence itself to the *Hoxa11* intron, the system whereby homeodomain transcription factor binding to the *Hoxa11* intron is restricted to HOXA13 was likely also introduced during the evolutionary transition from polydactyly to pentadactyly.

Figure 19

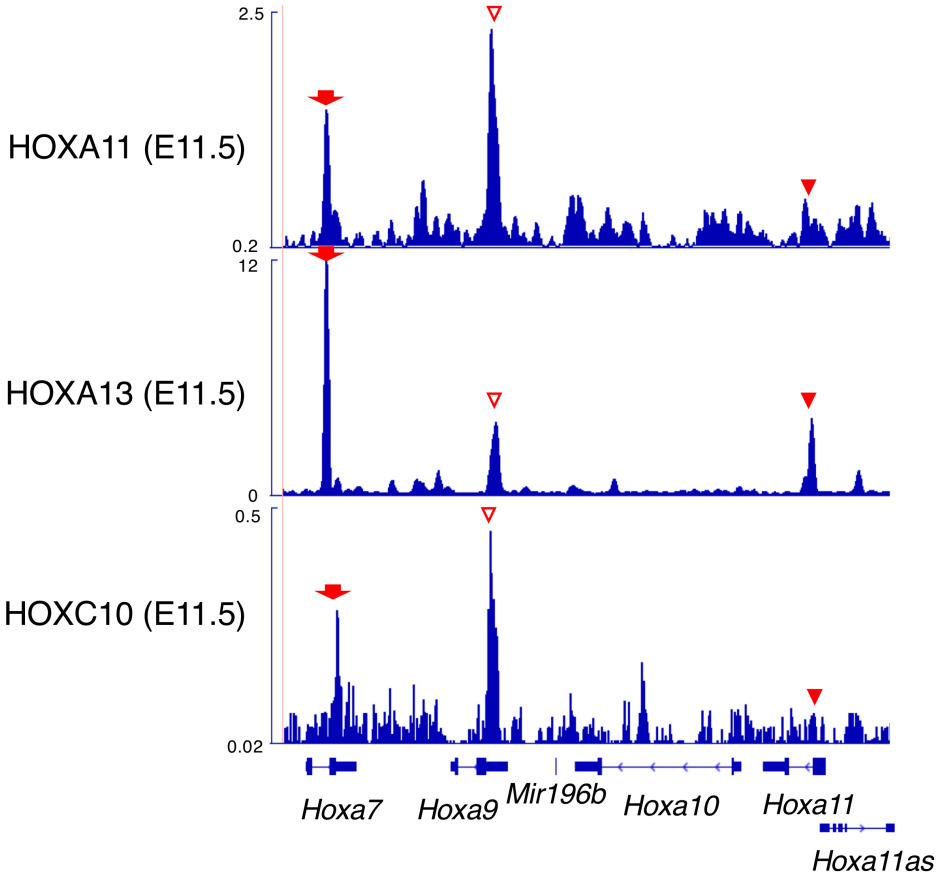

Fig. 19 Comparison of HOX binding profile in the *Hoxa7-Hoxa11* region.
HOXC10 binding profile in the E11.5 hindlimb bud was visualized by reanalysis of published data source presented in Table 6 using the same platform as for the HOX11/13 data. Arrow: intron of *Hoxa7*, open arrowhead: 5' UTR of *Hoxa9*, arrowhead: intron of *Hoxa11*. Numbers in the vertical axis indicate coverage values that were scaled by 1,000,000/total count.

Figure 20

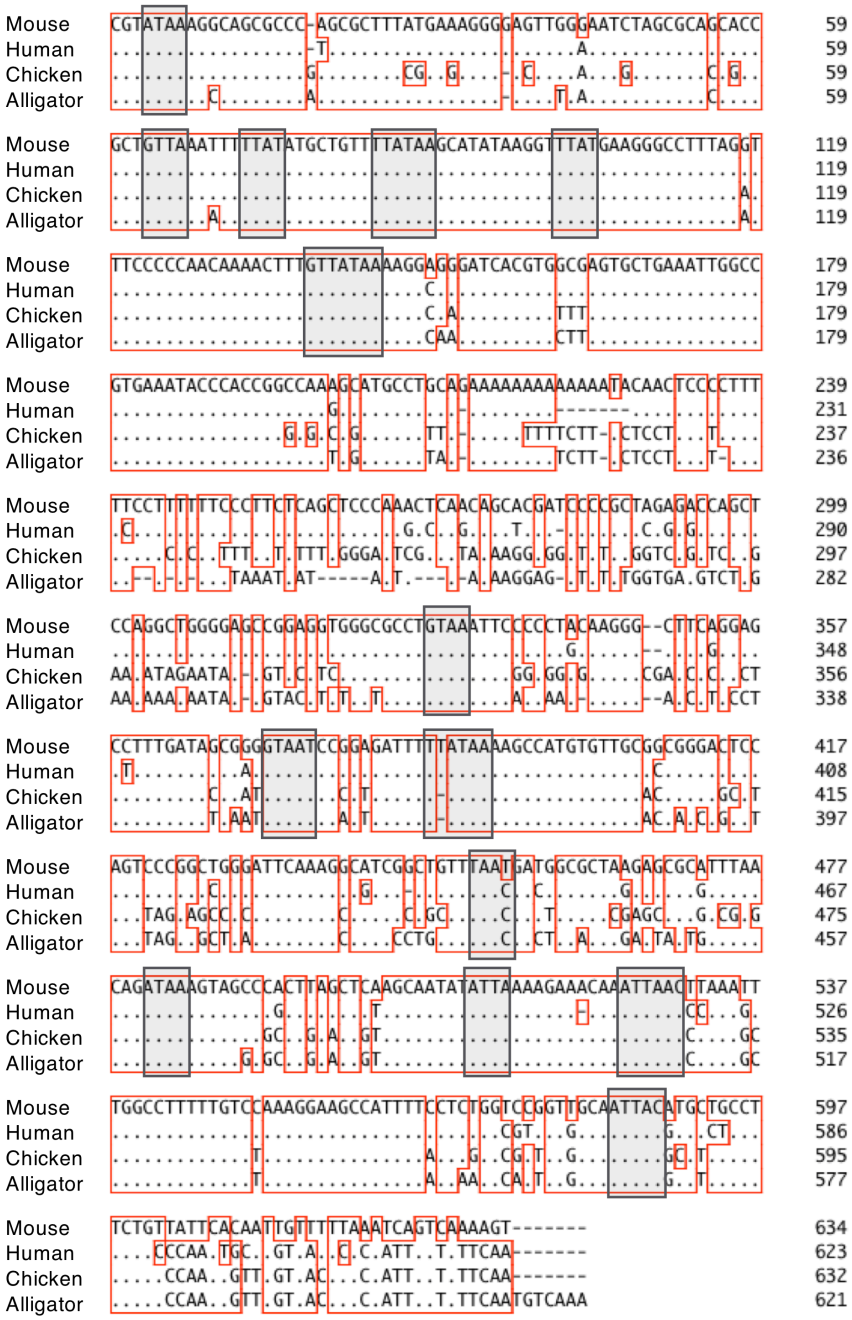

Fig. 20 Evolutionarily conserved multiple HBSs are present in the *Hoxa11* intronic region carrying mouse “digital enhancer”. Multiple HBSs (TTAT/C, TAAT/C: square) are conserved among the amniotes

The role of multiple HBSs in CHBRLs

It was shown that the sequences and the presence of multiple HBSs in most of the common ChIP-peaks of HOXA11 and HOXA13 (CHBRLNr) are evolutionarily conserved among tetrapods (Fig. 8, Fig. 9I-L and 20). The representative fragments exhibited direct binding of HOXA11 and HOXA13 to multiple binding sites *in vitro* (Fig. 8 and Fig. 9I-L) indicating that these HOX members may have similar binding profiles *in vivo*. Different from HOX1-10, HOXA11 and HOXA13 can bind to the target sequence without the co-factor homeodomain transcription factor, PBXs (Shen et al. 1997), and the most of the conserved HBSs in the CHBRLNr do not neighbor the consensus PBX binding sequence. Thus, it is likely that HOXA11 and HOXA13 solely bind their target sites. Since the clustered low affinity HBSs guarantee specificity and robustness of HOX binding in *Drosophila* (Crocker et al. 2015), multiple HOXA11 and HOXA13 binding sites in the vertebrate CHBRLNr should have the same role. This possibility is also supported by evidence that *Abd-B Hox* function shows a dosage effect on the patterning of limb cartilage (Zakany et al. 1997).

HOX function in the carpal/tarsal region

As already described, the relationship in the expression profile of *Hoxa11* and *Hoxa13* is unique. *Abd-B* family genes in the *HoxD* cluster, *Hoxd9-13,* maintain overlapping expression patterns in the limb bud, although transcription of *Hoxa11* is repressed in the distal limb bud by HOXA13 function. However, in the proximal region of the carpal/tarsal anlage, *Hoxa11* and *Hoxa13* maintain their co-expression despite the prominent expression of *Hoxa13* in the autopodal anlage (Fig. 1 and Fig. 2). Loss-of -function of either *Hoxa11* or *Hoxd11* also results in abnormal formation of the carpal/tarsal bones, similar to *Hox13* mutations indicating that *Hox11* has an additional role in the morphogenesis of the autopod other than just the zeugopod (Small and Potter 1993;Davis and Capecchi 1994;Fromental-Ramain et al. 1996). Cartilage formation in the carpal/tarsal region is unique compared to other limb regions. As shown in Fig.1 and Fig. 2, initially *Col2a1* expressing precartilaginous rudiment is formed in the prospective carpal/tarsal region, then multiple dense and small precartilaginous condensations

individualize as an archipelago. These precartilaginous condensations develop into cartilage and maintain the cartilaginous state for much longer than other regions and never develop into long bones. In contrast, in the prospective long bone forming regions, *Hoxa11* and *Hoxa13* exhibit mutually exclusive expression. It is possible that HOXA11 and HOXA13 co-exist in the regulatory region of the target gene carrying multiple HBSs in the carpal/tarsal anlage. This unique mixed state may enable the unique mode of cartilage differentiation in the carpal/tarsal region. It have been previously shown that mis-expression of *Hoxa13* in the zeugopodal region results in the transformation of the zeugopodal cartilage into the carpal/tarsal-like cartilage (Yokouchi et al. 1995), and this evidence further supports the hypothesis.

Regulation of *Hox* target genes by HOX

By this study, the genes neighboring the CHBRLNr were identified and it was demonstrated that their expression is changed in *Hox13*dKO embryos (Fig. 14, 15, 16 and 18), thus confirming them to be direct *Hox* target genes. These genes are classified into

two groups according to the changes in their mRNA levels in the *Hox13*dKO autopod. The genes in the first group showed reduced mRNA levels in the *Hox13*dKO, indicating that HOXA13 activates their transcription. The genes in the second group showed increased mRNA levels in the *Hox13*dKO and are likely repressed by HOXA13 during normal development.

Bmp2, *Sulf1* and *Stmn2* belong to the first group, and are expressed in the autopodal mesenchyme in wild-type animals and exhibited a substantial reduction in expression levels in the *Hox13*dKO embryos (Fig. 14 and Fig. 15). In the case of second gene group, expression of *Aff3*, *Bnc2*, *Nfib*, *Runx1t1, Shox2* and *Tshz2* are restricted to the zeugopodal mesenchyme of the wild-type embryos at E11.25-11.5, but showed ectopic expression in the autopod mesenchyme of *Hox13*dKO embryos (Fig. 14-16). Interestingly, the ectopic expression of *Aff3*, *Bnc2*, *Nfib* and *Runx1t1* was uniform in the *Hox13*dKO autopod, whereas *Shox2* mis-expression was restricted to a narrow posterior region of the *Hox13*dKO autopod and *Tshz2* mis-expression was only found in the distal autopod. These results indicate the presence of various mechanisms for HOXA13 negative

regulation of downstream genes.

The expression of *Hox* target genes, *Aff3*, *Bnc2* and *Nfib* is induced during cartilage differentiation, consistent with their known roles in cartilage differentiation (Uchihashi et al. 2007;Steichen-Gersdorf et al. 2008;Vanhoutteghem et al. 2009). As discussed above, the expression of these genes was not detected in the E11.5 autopodal anlage. Interestingly, these genes become expressed in the autopodal cartilage or perichondrium at E12.5 and sometimes even show partial overlapping expression with *Hoxa13*. Thus, repression of these genes by HOXA13 in the autopodal mesenchyme is transient during autopodal cartilage development. From E11.5 to E12.5 metacarpal/metatarsal and digital cartilage formation progresses distally and mesenchymal *Hoxa13* expression gradually decreases and disappears in the cartilage. During this period, in addition to the decreased amounts of HOXA13 protein, changes in the regulatory activity of HOXA13 may occur by modification of HOXA13 itself or by *de novo* induction of the HOXA13 co-factors that alter its transcriptional activity. Alternatively, since HOXA13 does not always bind to the H3K27ac enriched region of HOXA13 target genes, transitional usage of the enhancer

may occur between HOXA13 dependent regulatory elements and independent elements during cartilage differentiation from the limb mesenchyme. Enhancer switching during development has previously been demonstrated (Andrey et al. 2013;Beccari et al. 2016;Glasgow et al. 2017), thus it is possible that a similar system is employed during cartilage differentiation.

In contrast to autopodal expression, these *Hox* target genes are also expressed in the zeugopodal mesenchyme prior to their cartilage expression and exhibit nearly complete overlap with *Hoxa11* expression. This suggests that the mechanisms underlying HOXA11-dependent and HOXA13-dependent gene regulations are different.

HOX13 regulates cartilage differentiation in a dual manner

In contrast to the genes encoding transcription factors that are enriched among the *Hox* targets with upregulated expression in the *Hox13*dKO limb bud (Fig. 13), relatively few *Hox* target transcription factors were identified in the downregulated fraction (Fig. 13). A typical example of the latter case is *Bcl11a*. *Bcl11a* encodes a zinc finger-type

transcription factor and functions as a repressor during blood cell differentiation (Liu et al. 2003). It was found that *Bcl11a* along with its family member *Bcl11b*, repressed cartilage differentiation from the limb bud mesenchyme (Fig. 18).

In the *Hox13*dKO autopod, the entire autopodal mesenchyme excluding the distal most region, enters the cartilage differentiation pathway earlier than during normal development. *Bcl11a* is expressed in the autopodal mesenchyme in the wild-type E11.5 embryos and its expression is substantially reduced in the *Hox13*dKO limb bud (Fig. 18B,C). This indicates that the cartilage differentiation program repressed by HOXA13 is de-repressed in the *Hox13*dKO autopod. Simultaneously, the *Hox* target transcription factors whose expression is induced during cartilage differentiation, are mis-expressed in the mesenchyme of the *Hox13*dKO autopodal anlage. Combined, these results indicate that HOXA13 simultaneously activates the expression of repressive transcription factors for chondrogenesis (BCL11A) and represses the expression of transcription factors required to induce chondrogenesis in the autopod at E11.5. This demonstrates the presence of a dual regulatory mechanism for chondrogenesis during normal autopod

development under the control of *Hoxa13*. In contrast to the autopod, *Hoxa11* and *Hox* target genes such as *Aff3*, *Bnc2*, *Nfib*, Shox2 and *Runx1t1*, are co-expressed in the zeugopodal mesenchyme. This implies that, different from HOXA13, HOXA11 does not repress the expression of these target genes. Thus, the HOXA13-dependent dual control system is autopod-specific.

Regarding the genes not expressed in the autopodal mesenchyme at E11.5 but that are mis-expressed in the *Hox13*dKO, it was proposed that HOXA13 may repress these genes during normal development. However, the following mechanism is equally probable; for these target genes, HOX13 may function as a weaker transcriptional activator than HOX11. The evidence that limb mesenchymal cells isolated from Hoxa13$^{-/-}$ embryos did not show cartilage differentiation *in vitro* support that HOXA13 is required for cartilage differentiation (Stadler et al. 2001). If repressive transcription factor(s) for the *Hox* target gene expression are present in the E11.5 autopodal mesenchyme, and transcriptional activation by HOX13 does not overcome this repressive activity, the autopodal expression of the *Hox* target gene does not occur. *Hoxa11* and *Hoxa13*

exhibited mutually exclusive expression in the limb bud except in the carpal/tarsal anlage; however, in the *Hox13*dKO autopod, *Hoxa11* expression is expanded to the autopodal mesenchyme (Sheth et al. 2014). This ectopic HOXA11 may mis-activate the common *Hox* target genes required for cartilage differentiation in the *Hox13*dKO autopod. The evidence that the forced mis-expression of *Hoxa11* in the autopod results in polydactyly supports this possibility (Kherdjemil et al. 2016). Expression analysis of common *Hox* target genes in the autopod under *Hoxa11* mis-expression may help to verify this mechanism.

The molecular mechanism that is responsible for the dual transcriptional activity of HOXA13 presented here, along with the similar effect of HOXA13 on *HoxD* gene expression shown by Beccari et al. (Beccari et al. 2016), remains elusive. Recently it is reported that a transcription factor that shows unique spatiotemporal expression patterns, interacts with HOX in a DNA binding dependent or independent manner, then modulates the function of HOX transcription factors (Guerreiro et al. 2013). In the case of *Drosophila*, the phosphorylation state of the HOX protein is crucial for its transcriptional activity (Berry

and Gehring 2000). In addition, the presence of the co-factors that modulate transcriptional activity of *Drosophila* HOX was reported (reviewed in (Zandvakili and Gebelein 2016)). Since these mechanisms related to HOXA13 have yet to be elucidated, research into this issue will be a topic for future studies.

Hox13 **controls tetrapod specific autopodal structure**

Why does *Hoxa13*, the last member of the *HoxA* cluster, have such unique function compared to other *Hox* genes expressed in the zeugopod or stylopod? This is likely related to the development of tetrapod-specific autopodal structures. In contrast to the zeugopod and stylopod, the autopod generally consists of five sets of long bones, the metacarpi/metatarsi and phalanges (pentadactyly). One and two long bones exist in the stylopod and zeugopod, respectively, and the shape of their prospective region in the limb bud is a nearly elliptical cylinder. In contrast, the autopodal anlage has a unique paddle-shaped structure that is required for supplying a sufficient number of mesenchymal cells to generate the pentadactylous cartilage pattern. The signaling factor, SHH, expressed in

the mesenchyme of the posterior limb bud, is essential for expansion of the autopodal anlage (Chiang et al. 1996) and *Hox13* directly activates *Shh* expression via a limb enhancer (Leal and Cohn 2016;Leal and Cohn 2018). In addition, another signaling molecule, *Fgf10*, expressed in the distal limb bud, is required for limb bud formation and growth (Sekine et al. 1999). *Abd-B Hox* is also involved in activating *Fgf10* expression in the limb bud (Sheth et al. 2013) and it was found that HOXA11 and HOXA13 bind one of the *Fgf10* limb enhancers (VISTA ID mm917, Table 2). Thus, *Hox13* positively controls the proliferation of autopodal mesenchymal cells to supply sufficient number of mesenchymal cells to generate the pentadactylous autopodal cartilage pattern. As discussed above, HOX13 transiently represses the cartilage differentiation program in the autopodal anlage in a dual manner. Thus, *Hox13* functions on one hand to control the autopod-specific growth program to supply enough mesenchyme and, on the other hand, transiently represses the cartilage forming program until the mesenchymal supply reaches a sufficient level to form pentadactylous structures (Fig. 21).

The pentadactylous autopodal architecture is unique to the tetrapods and this basic

architectural design was key to tetrapod evolution through niche diversification. Recently, in fish, *Hox13* genes were shown to function in switching the fin bud mesenchymal developmental program from cartilage formation to fin ray differentiation (Nakamura et al. 2016). In the case of pentadactylous tetrapods, *Hox13* function switched from the fish program to the tetrapod-specific autopod-forming program, possibly through the acquisition of the dual control system for cartilage differentiation.

Figure 21

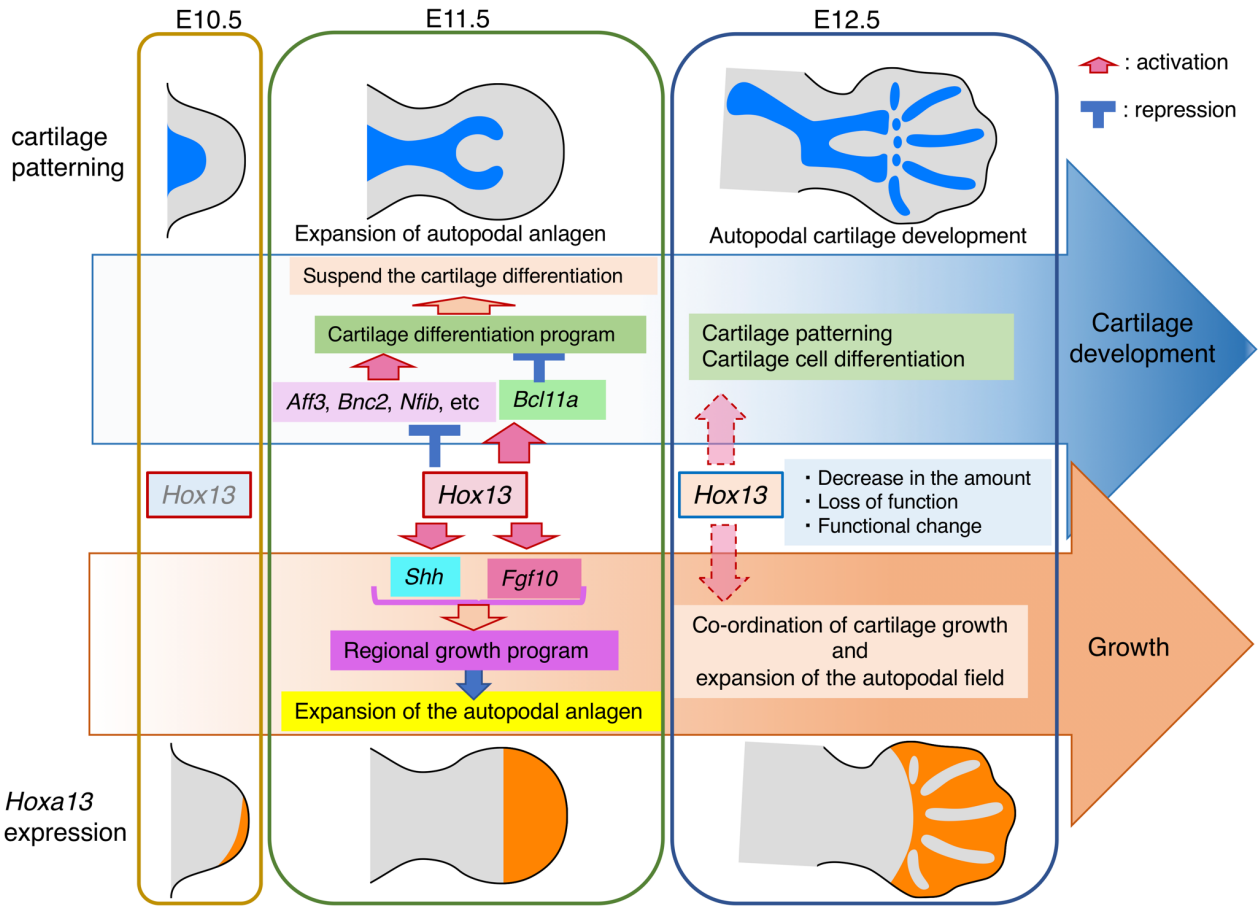

Fig. 21 Dynamic change in the *Hoxa13* function during autopod development

Acknowledgements

Drs. N. Yakushiji-Kaminatsui, T. Higashiyama and T. Suzuki for a part of NGS analysis.

Dr. T. Takemoto for generating CisKO mice.

Drs. K. Ihara, S. Oki and N. Nakamichi for assistance with bioinformatic data analysis.

Dr. S. Pastuhov for assistance with quantification of Col II expression.

Drs. P. Chambon and D. Duboule for the *Hox* KO mice.

Shiori Yamamoto was supported by the “Integrative Graduate Education and Research in Green Natural Sciences” program (Ministry of Education, Culture, Sports, Science and Technology, Japan).

References

Andrey, G., Montavon, T., Mascrez, B., Gonzalez, F., Noordermeer, D., Leleu, M., Trono, D., Spitz, F. and Duboule, D. 2013. A switch between topological domains underlies HoxD genes collinearity in mouse limbs. *Science* **340**, 1234167.

Beccari, L., Yakushiji-Kaminatsui, N., Woltering, J. M., Necsulea, A., Lonfat, N., Rodriguez-Carballo, E., Mascrez, B., Yamamoto, S., Kuroiwa, A. and Duboule, D. 2016. A role for HOX13 proteins in the regulatory switch between TADs at the HoxD locus. *Genes Dev* **30**, 1172-1186.

Berry, M. and Gehring, W. 2000. Phosphorylation status of the SCR homeodomain determines its functional activity: essential role for protein phosphatase 2A,B'. *EMBO J* **19**, 2946-2957.

Bobick, B. E. and Cobb, J. 2012. Shox2 regulates progression through chondrogenesis in the mouse proximal limb. *J Cell Sci* **125**, 6071-6083.

Boulet, A. M. and Capecchi, M. R. 2004. Multiple roles of Hoxa11 and Hoxd11 in the formation of the mammalian forelimb zeugopod. *Development* **131**, 299-309.

Buscher, D., Bosse, B., Heymer, J. and Ruther, U. 1997. Evidence for genetic control of Sonic hedgehog by Gli3 in mouse limb development. *Mech Dev* **62**, 175-182.

Capellini, T. D., Di Giacomo, G., Salsi, V., Brendolan, A., Ferretti, E., Srivastava, D., Zappavigna, V. and Selleri, L. 2006. Pbx1/Pbx2 requirement for distal limb patterning is mediated by the hierarchical control of Hox gene spatial distribution and Shh expression. *Development* **133**, 2263-2273.

Caubit, X., Core, N., Boned, A., Kerridge, S., Djabali, M. and Fasano, L. 2000. Vertebrate orthologues of the Drosophila region-specific patterning gene teashirt. *Mech Dev* **91**, 445-448.

Chen, Y., Knezevic, V., Ervin, V., Hutson, R., Ward, Y. and Mackem, S. 2004. Direct interaction with Hoxd proteins reverses Gli3-repressor function to promote digit formation downstream of Shh. *Development* **131**, 2339-2347.

Chiang, C., Litingtung, Y., Lee, E., Young, K. E., Corden, J. L., Westphal, H. and Beachy, P. A. 1996. Cyclopia and defective axial patterning in mice lacking Sonic hedgehog gene function. *Nature* **383**, 407-413.

Cobb, J., Dierich, A., Huss-Garcia, Y. and Duboule, D. 2006. A mouse model for human short-stature syndromes identifies Shox2 as an upstream regulator of Runx2 during long-bone development. *Proc Natl Acad Sci U S A* **103**, 4511-4515.
Crocker, J., Abe, N., Rinaldi, L., McGregor, A. P., Frankel, N., Wang, S., Alsawadi, A., Valenti, P., Plaza, S., Payre, F., Mann, R. S. and Stern, D. L. 2015. Low affinity binding site clusters confer hox specificity and regulatory robustness. *Cell* **160**, 191-203.
Dathe, K., Kjaer, K. W., Brehm, A., Meinecke, P., Nurnberg, P., Neto, J. C., Brunoni, D., Tommerup, N., Ott, C. E., Klopocki, E., Seemann, P. and Mundlos, S. 2009. Duplications involving a conserved regulatory element downstream of BMP2 are associated with brachydactyly type A2. *Am J Hum Genet* **84**, 483-492.
Davis, A. P. and Capecchi, M. R. 1994. Axial homeosis and appendicular skeleton defects in mice with a targeted disruption of hoxd-11. *Development* **120**, 2187-2198.
Davis, A. P., Witte, D. P., Hsieh-Li, H. M., Potter, S. S. and Capecchi, M. R. 1995. Absence of radius and ulna in mice lacking hoxa-11 and hoxd-11. *Nature* **375**, 791-795.
Dickinson, M. E., Kobrin, M. S., Silan, C. M., Kingsley, D. M., Justice, M. J., Miller, D. A., Ceci, J. D., Lock, L. F., Lee, A., Buchberg, A. M. and et al. 1990. Chromosomal localization of seven members of the murine TGF-beta superfamily suggests close linkage to several morphogenetic mutant loci. *Genomics* **6**, 505-520.
Fromental-Ramain, C., Warot, X., Messadecq, N., LeMeur, M., Dolle, P. and Chambon, P. 1996. Hoxa-13 and Hoxd-13 play a crucial role in the patterning of the limb autopod. *Development* **122**, 2997-3011.
Giardine, B., Riemer, C., Hardison, R. C., Burhans, R., Elnitski, L., Shah, P., Zhang, Y., Blankenberg, D., Albert, I., Taylor, J., Miller, W., Kent, W. J. and Nekrutenko, A. 2005. Galaxy: a platform for interactive large-scale genome analysis. *Genome Res* **15**, 1451-1455.
Gilbert, S. F. and Barresi, M. J. F. 2016. *Developmental Biology*. Sunderland, Massachusetts, U.S.A., Sinauer Associates, Inc.
Glasgow, S. M., Carlson, J. C., Zhu, W., Chaboub, L. S., Kang, P., Lee, H. K., Clovis, Y. M., Lozzi, B. E., McEvilly, R. J., Rosenfeld, M. G., Creighton, C. J., Lee, S. K., Mohila, C. A. and Deneen, B. 2017. Glia-specific enhancers and chromatin structure regulate NFIA expression and glioma tumorigenesis. *Nat Neurosci* **20**, 1520-1528.

Goff, D. J. and Tabin, C. J. 1997. Analysis of Hoxd-13 and Hoxd-11 misexpression in chick limb buds reveals that Hox genes affect both bone condensation and growth. *Development* **124**, 627-636.
Green, M. R. and Sambrook, J., Eds. (2012). Molecular Cloning: A Laboratory Manual (Fourth edition). Cold Spring Harbor, New York, Cold Spring Harbor Laboratory Press.
Gross, S., Krause, Y., Wuelling, M. and Vortkamp, A. 2012. Hoxa11 and Hoxd11 regulate chondrocyte differentiation upstream of Runx2 and Shox2 in mice. *PLoS One* **7**, e43553.
Guerreiro, I., Nunes, A., Woltering, J. M., Casaca, A., Novoa, A., Vinagre, T., Hunter, M. E., Duboule, D. and Mallo, M. 2013. Role of a polymorphism in a Hox/Pax-responsive enhancer in the evolution of the vertebrate spine. *Proc Natl Acad Sci U S A* **110**, 10682-10686.
Hashimoto, M., Yamashita, Y. and Takemoto, T. 2016. Electroporation of Cas9 protein/sgRNA into early pronuclear zygotes generates non-mosaic mutants in the mouse. *Dev Biol* **418**, 1-9.
Huang da, W., Sherman, B. T. and Lempicki, R. A. 2009. Systematic and integrative analysis of large gene lists using DAVID bioinformatics resources. *Nat Protoc* **4**, 44-57.
Izpisua-Belmonte, J. C., Tickle, C., Dolle, P., Wolpert, L. and Duboule, D. 1991. Expression of the homeobox Hox-4 genes and the specification of position in chick wing development. *Nature* **350**, 585-589.
Jain, D., Nemec, S., Luxey, M., Gauthier, Y., Bemmo, A., Balsalobre, A. and Drouin, J. 2018. Regulatory integration of Hox factor activity with T-box factors in limb development. *Development* **145**,
Jerkovic, I., Ibrahim, D. M., Andrey, G., Haas, S., Hansen, P., Janetzki, C., Gonzalez Navarrete, I., Robinson, P. N., Hecht, J. and Mundlos, S. 2017. Genome-Wide Binding of Posterior HOXA/D Transcription Factors Reveals Subgrouping and Association with CTCF. *PLoS Genet* **13**, e1006567.
Karolchik, D., Hinrichs, A. S., Furey, T. S., Roskin, K. M., Sugnet, C. W., Haussler, D. and Kent, W. J. 2004. The UCSC Table Browser data retrieval tool. *Nucleic Acids Res* **32**, D493-496.
Kherdjemil, Y., Lalonde, R. L., Sheth, R., Dumouchel, A., de Martino, G., Pineault, K. M., Wellik, D. M., Stadler, H. S., Akimenko, M. A. and Kmita, M. 2016. Evolution of Hoxa11

regulation in vertebrates is linked to the pentadactyl state. *Nature* **539**, 89-92.
Kmita, M., Tarchini, B., Zakany, J., Logan, M., Tabin, C. J. and Duboule, D. 2005. Early developmental arrest of mammalian limbs lacking HoxA/HoxD gene function. *Nature* **435**, 1113-1116.
Lanctot, C., Moreau, A., Chamberland, M., Tremblay, M. L. and Drouin, J. 1999. Hindlimb patterning and mandible development require the Ptx1 gene. *Development* **126**, 1805-1810.
Langmead, B. and Salzberg, S. L. 2012. Fast gapped-read alignment with Bowtie 2. *Nat Methods* **9**, 357-359.
Leal, F. and Cohn, M. J. 2016. Loss and Re-emergence of Legs in Snakes by Modular Evolution of Sonic hedgehog and HOXD Enhancers. *Curr Biol* **26**, 2966-2973.
Leal, F. and Cohn, M. J. 2018. Developmental, genetic, and genomic insights into the evolutionary loss of limbs in snakes. *Genesis* **56**, e23077.
Lewandowski, J. P., Du, F., Zhang, S., Powell, M. B., Falkenstein, K. N., Ji, H. and Vokes, S. A. 2015. Spatiotemporal regulation of GLI target genes in the mammalian limb bud. *Dev Biol* **406**, 92-103.
Liu, P., Keller, J. R., Ortiz, M., Tessarollo, L., Rachel, R. A., Nakamura, T., Jenkins, N. A. and Copeland, N. G. 2003. Bcl11a is essential for normal lymphoid development. *Nat Immunol* **4**, 525-532.
Long, H. K., Prescott, S. L. and Wysocka, J. 2016. Ever-Changing Landscapes: Transcriptional Enhancers in Development and Evolution. *Cell* **167**, 1170-1187.
Machanick, P. and Bailey, T. L. 2011. MEME-ChIP: motif analysis of large DNA datasets. *Bioinformatics* **27**, 1696-1697.
McCabe, C. D. and Innis, J. W. 2005. A genomic approach to the identification and characterization of HOXA13 functional binding elements. *Nucleic Acids Res* **33**, 6782-6794.
McLean, C. Y., Bristor, D., Hiller, M., Clarke, S. L., Schaar, B. T., Lowe, C. B., Wenger, A. M. and Bejerano, G. 2010. GREAT improves functional interpretation of cis-regulatory regions. *Nat Biotechnol* **28**, 495-501.
Mi, H., Muruganujan, A. and Thomas, P. D. 2013. PANTHER in 2013: modeling the evolution of gene function, and other gene attributes, in the context of phylogenetic

trees. *Nucleic Acids Res* **41**, D377-386.
Nakamura, T., Gehrke, A. R., Lemberg, J., Szymaszek, J. and Shubin, N. H. 2016. Digits and fin rays share common developmental histories. *Nature* **537**, 225-228.
Nemec, S., Luxey, M., Jain, D., Huang Sung, A., Pastinen, T. and Drouin, J. 2017. Pitx1 directly modulates the core limb development program to implement hindlimb identity. *Development* **144**, 3325-3335.
Neufeld, S. J., Wang, F. and Cobb, J. 2014. Genetic interactions between Shox2 and Hox genes during the regional growth and development of the mouse limb. *Genetics* **198**, 1117-1126.
Oki, S., Maehara, K., Ohkawa, Y. and Meno, C. 2014. SraTailor: graphical user interface software for processing and visualizing ChIP-seq data. *Genes Cells* **19**, 919-926.
Osterwalder, M., Barozzi, I., Tissieres, V., Fukuda-Yuzawa, Y., Mannion, B. J., Afzal, S. Y., Lee, E. A., Zhu, Y., Plajzer-Frick, I., Pickle, C. S., Kato, M., Garvin, T. H., Pham, Q. T., Harrington, A. N., Akiyama, J. A., Afzal, V., Lopez-Rios, J., Dickel, D. E., Visel, A. and Pennacchio, L. A. 2018. Enhancer redundancy provides phenotypic robustness in mammalian development. *Nature* **554**, 239-243.
Peichel, C. L., Prabhakaran, B. and Vogt, T. F. 1997. The mouse Ulnaless mutation deregulates posterior HoxD gene expression and alters appendicular patterning. *Development* **124**, 3481-3492.
Pineault, K. M. and Wellik, D. M. 2014. Hox genes and limb musculoskeletal development. *Curr Osteoporos Rep* **12**, 420-427.
Quinlan, A. R. and Hall, I. M. 2010. BEDTools: a flexible suite of utilities for comparing genomic features. *Bioinformatics* **26**, 841-842.
Ramirez, F., Ryan, D. P., Gruning, B., Bhardwaj, V., Kilpert, F., Richter, A. S., Heyne, S., Dundar, F. and Manke, T. 2016. deepTools2: a next generation web server for deep-sequencing data analysis. *Nucleic Acids Res* **44**, W160-165.
Robinson, J. T., Thorvaldsdottir, H., Winckler, W., Guttman, M., Lander, E. S., Getz, G. and Mesirov, J. P. 2011. Integrative genomics viewer. *Nat Biotechnol* **29**, 24-26.
Rosin, J. M., Abassah-Oppong, S. and Cobb, J. 2013. Comparative transgenic analysis of enhancers from the human SHOX and mouse Shox2 genomic regions. *Hum Mol Genet* **22**, 3063-3076.

Salsi, V. and Zappavigna, V. 2006. Hoxd13 and Hoxa13 directly control the expression of the EphA7 Ephrin tyrosine kinase receptor in developing limbs. *J Biol Chem* **281**, 1992-1999.
Sekine, K., Ohuchi, H., Fujiwara, M., Yamasaki, M., Yoshizawa, T., Sato, T., Yagishita, N., Matsui, D., Koga, Y., Itoh, N. and Kato, S. 1999. Fgf10 is essential for limb and lung formation. *Nat Genet* **21**, 138-141.
Selleri, L., Depew, M. J., Jacobs, Y., Chanda, S. K., Tsang, K. Y., Cheah, K. S., Rubenstein, J. L., O'Gorman, S. and Cleary, M. L. 2001. Requirement for Pbx1 in skeletal patterning and programming chondrocyte proliferation and differentiation. *Development* **128**, 3543-3557.
Shang, J., Luo, Y. and Clayton, D. A. 1997. Backfoot is a novel homeobox gene expressed in the mesenchyme of developing hind limb. *Dev Dyn* **209**, 242-253.
Shen, W. F., Rozenfeld, S., Lawrence, H. J. and Largman, C. 1997. The Abd-B-like Hox homeodomain proteins can be subdivided by the ability to form complexes with Pbx1a on a novel DNA target. *J Biol Chem* **272**, 8198-8206.
Sheth, R., Barozzi, I., Langlais, D., Osterwalder, M., Nemec, S., Carlson, H. L., Stadler, H. S., Visel, A., Drouin, J. and Kmita, M. 2016. Distal Limb Patterning Requires Modulation of cis-Regulatory Activities by HOX13. *Cell Rep* **17**, 2913-2926.
Sheth, R., Bastida, M. F., Kmita, M. and Ros, M. 2014. "Self-regulation," a new facet of Hox genes' function. *Dev Dyn* **243**, 182-191.
Sheth, R., Gregoire, D., Dumouchel, A., Scotti, M., Pham, J. M., Nemec, S., Bastida, M. F., Ros, M. A. and Kmita, M. 2013. Decoupling the function of Hox and Shh in developing limb reveals multiple inputs of Hox genes on limb growth. *Development* **140**, 2130-2138.
Shin, H., Liu, T., Manrai, A. K. and Liu, X. S. 2009. CEAS: cis-regulatory element annotation system. *Bioinformatics* **25**, 2605-2606.
Small, K. M. and Potter, S. S. 1993. Homeotic transformations and limb defects in Hox A11 mutant mice. *Genes Dev* **7**, 2318-2328.
Stadler, H. S., Higgins, K. M. and Capecchi, M. R. 2001. Loss of Eph-receptor expression correlates with loss of cell adhesion and chondrogenic capacity in Hoxa13 mutant limbs. *Development* **128**, 4177-4188.

Steichen-Gersdorf, E., Gassner, I., Superti-Furga, A., Ullmann, R., Stricker, S., Klopocki, E. and Mundlos, S. 2008. Triangular tibia with fibular aplasia associated with a microdeletion on 2q11.2 encompassing LAF4. *Clin Genet* **74**, 560-565.
Swinehart, I. T., Schlientz, A. J., Quintanilla, C. A., Mortlock, D. P. and Wellik, D. M. 2013. Hox11 genes are required for regional patterning and integration of muscle, tendon and bone. *Development* **140**, 4574-4582.
Szeto, D. P., Rodriguez-Esteban, C., Ryan, A. K., O'Connell, S. M., Liu, F., Kioussi, C., Gleiberman, A. S., Izpisua-Belmonte, J. C. and Rosenfeld, M. G. 1999. Role of the Bicoid-related homeodomain factor Pitx1 in specifying hindlimb morphogenesis and pituitary development. *Genes Dev* **13**, 484-494.
Uchihashi, T., Kimata, M., Tachikawa, K., Koshimizu, T., Okada, T., Ihara-Watanabe, M., Sakai, N., Kogo, M., Ozono, K. and Michigami, T. 2007. Involvement of nuclear factor I transcription/replication factor in the early stage of chondrocytic differentiation. *Bone* **41**, 1025-1035.
Vanhoutteghem, A., Maciejewski-Duval, A., Bouche, C., Delhomme, B., Herve, F., Daubigney, F., Soubigou, G., Araki, M., Araki, K., Yamamura, K. and Djian, P. 2009. Basonuclin 2 has a function in the multiplication of embryonic craniofacial mesenchymal cells and is orthologous to disco proteins. *Proc Natl Acad Sci U S A* **106**, 14432-14437.
Visel, A., Minovitsky, S., Dubchak, I. and Pennacchio, L. A. 2007. VISTA Enhancer Browser--a database of tissue-specific human enhancers. *Nucleic Acids Res* **35**, D88-92.
Vokes, S. A., Ji, H., Wong, W. H. and McMahon, A. P. 2008. A genome-scale analysis of the cis-regulatory circuitry underlying sonic hedgehog-mediated patterning of the mammalian limb. *Genes Dev* **22**, 2651-2663.
Yamamoto, M., Gotoh, Y., Tamura, K., Tanaka, M., Kawakami, A., Ide, H. and Kuroiwa, A. 1998. Coordinated expression of *Hoxa-11* and *Hoxa-13* during limb muscle patterning. *Development* **125**, 1325-1335.
Yamamoto-Shiraishi, Y., Higuchi, H., Yamamoto, S., Hirano, M. and Kuroiwa, A. 2014. Etv1 and Ewsr1 cooperatively regulate limb mesenchymal Fgf10 expression in response to apical ectodermal ridge-derived fibroblast growth factor signal. *Dev Biol* **394**, 181-190.
Yamamoto-Shiraishi, Y. and Kuroiwa, A. 2013. Wnt and BMP signaling cooperate with

Hox in the control of Six2 expression in limb tendon precursor. *Dev Biol* **377**, 363-374.
Ye, W., Song, Y., Huang, Z., Osterwalder, M., Ljubojevic, A., Xu, J., Bobick, B., Abassah-Oppong, S., Ruan, N., Shamby, R., Yu, D., Zhang, L., Cai, C. L., Visel, A., Zhang, Y., Cobb, J. and Chen, Y. 2016. A unique stylopod patterning mechanism by Shox2-controlled osteogenesis. *Development* **143**, 2548-2560.
Yokouchi, Y., Nakazato, S., Yamamoto, M., Goto, Y., Kameda, T., Iba, H. and Kuroiwa, A. 1995. Misexpression of Hoxa-13 induces cartilage homeotic transformation and changes cell adhesiveness in chick limb buds. *Genes Dev* **9**, 2509-2522.
Yokouchi, Y., Sasaki, H. and Kuroiwa, A. 1991. Homeobox gene expression correlated with the bifurcation process of limb cartilage development. *Nature* **353**, 443-445.
Yue, F. et al. 2014. A comparative encyclopedia of DNA elements in the mouse genome. *Nature* **515**, 355-364.
Zakany, J., Fromental-Ramain, C., Warot, X. and Duboule, D. 1997. Regulation of number and size of digits by posterior Hox genes: a dose-dependent mechanism with potential evolutionary implications. *Proc Natl Acad Sci U S A* **94**, 13695-13700.
Zakany, J., Zacchetti, G. and Duboule, D. 2007. Interactions between HOXD and Gli3 genes control the limb apical ectodermal ridge via Fgf10. *Dev Biol* **306**, 883-893.
Zandvakili, A. and Gebelein, B. 2016. Mechanisms of Specificity for Hox Factor Activity. *J Dev Biol* **4**,
Zhang, Y., Liu, T., Meyer, C. A., Eeckhoute, J., Johnson, D. S., Bernstein, B. E., Nusbaum, C., Myers, R. M., Brown, M., Li, W. and Liu, X. S. 2008. Model-based analysis of ChIP-Seq (MACS). *Genome Biol* **9**, R137.

Table legends

Table 1a: Peak numbers of the E11.5 individual HOXA11 and HOXA13 peaks and common peak numbers.

Table 1b: Intersecting peak numbers and Bed file.

Table 2: Profiling of the CHBRLNr genes. The colored cell indicates the gene near the overlapping peak.

Table 3a: Genechip analysis detecting changes in E11.25 autopodal gene expression in the *Hox13*dKO.

Table 3b: List of the genes exhibiting expression change in the *Hox13*dKO autopod at E11.25.

Table 3c: List of the genes categorized under “transcription regulation” in the “upregulated” CHBRLNr genes.

Table 4: List of the genes in the CHBRLNr containing TAD.

Identification of the genes present in the TAD that carry CHBRLNr

First, a new TAD bed file was created by combining two sets of mESC HindIII TAD (rep1

and rep2, 2200 regions). Then the TAD containing a11a13_100Nr (1518 regions) was selected using BED Tools (“intersect intervals”) of Galaxy (1456 regions). Using this TAD bed file and UCSCRefSEQ, 19049 exonic regions including the selected TAD were extracted then genes carrying these exons were identified (6191 genes). 1562 genes flanking the CHBRLNr were identified by GREAT analysis. Among these, 1232 genes (79%) were matched to the a11a13TAD genes indicating that most of the genes identified by GREAT have the CHBRLNr in the same TAD.

Table 5a-f: Information on primer sequences and *cis*KO

Table 6: List of data sets obtained from public databases